General Disclaimer

One or more of the Following Statements may affect this Document

- This document has been reproduced from the best copy furnished by the organizational source. It is being released in the interest of making available as much information as possible.

- This document may contain data, which exceeds the sheet parameters. It was furnished in this condition by the organizational source and is the best copy available.

- This document may contain tone-on-tone or color graphs, charts and/or pictures, which have been reproduced in black and white.

- This document is paginated as submitted by the original source.

- Portions of this document are not fully legible due to the historical nature of some of the material. However, it is the best reproduction available from the original submission.

A SIMULATION STUDY OF ACTIVE FEEDBACK SUPPRESSION OF DYNAMIC RESPONSE IN HELICOPTER ROTOR BLADES

Daniel D. Kana

Roger L. Bessey

Franklin T. Dodge
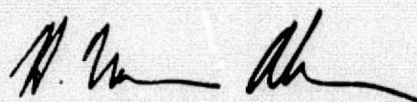
FINAL REPORT
Contract No. NAS1-12974
SwRI Project No. 02-3893

July 1, 1975

Approved:

_____

H. Norman Abramson,
Vice President, Engineering Sciences

TABLE OF CONTENTS

AERODYNAMIC MATHEMATICAL MODEL

Definition of the Problem

To study active control of the aeroelastic response of rotor blades to gust or discrete pulse loadings, an analytical aerodynamic model is needed which allows concentrated loadings to be applied in a general way. The model should also be in a form suitable for use with the electromechanical analog used in the experimental simulation study.

Aerodynamic strip theory is a convenient way to formulate a model that allows for general spanwise and timewise loads. To use strip theory, three-dimensional effects (for example, spanwise aerodynamic derivatives) must be neglected. The basic relations between the unsteady blade motions and the unsteady air flow are derived from quasi-steady aerodynamic theory. This is equivalent to assuming that the actual unsteady, Theodorsen-like aerodynamic load functions are replaced by unity in the lift and moment equations of strip theory (Ref. 1). There is a controversy in the literature about the aerodynamic damping coefficient derived by this approximation (Ref. 2), but the approximation is certainly used widely. The unsteady effects of the rotor wake are ignored, which is a necessity in any case because a tractable description of the wake aerodynamics is lacking.

Specific Assumptions

In addition to the use of quasi-steady strip theory, a number of specific assumptions are made in developing the mathematical model. For convenient reference, these are listed below as a group.

1. Spanwise velocities do not make a direct contribution to lift or drag.

2. The induced downwash and the component of the forward flight velocity normal to the rotor disk are both small relative either to the tip rotational speed or to the forward velocity.

3. The shaft tilt angle α_s is small, so that $\sin \alpha_s = \alpha_s$ and $\cos \alpha_s = 1$.

4. The bending, flapping, and torsional deflections are so small that products of them with other small quantities are negligible.

3

5. Cyclic pitch θ_c is small, so that $\sin \theta_c = \theta_c$ and $\cos \theta_c = 1$.

6. The slope of the lift-coefficient versus α_r curve for reversed flow is the same as for forward flight, for the unstalled flight regimes.

7. Blade stall is confined to blade sections and azimuth angles where the chordwise velocity is close to zero. Loads due to stall effects, therefore, can be neglected because of the smallness of the dynamic pressure in the stalled region.

8. The rate of climb is zero.

The aerodynamic assumptions are justified in Reference 3. Assumption No. 6 is a good approximation for typical symmetric airfoil sections (such as NACA 0012) used for helicopters, when the angle of attack is below stall. With regard to Assumption No. 7, the angle of attack at a section varies from non-stalled positive values to zero, and then very rapidly through the range of large values of angle of attack (i.e., stall) as the chordwise velocity varies from a small forward value to a small rearward value; in the region where the chordwise velocity has a large rearward value, the angle of attack is near $-\pi$ and the blade section is again unstalled according to Assumption No. 6.

In the light of these assumptions, no pretense is made that the model is "exact" or likely to be of value for flutter analyses and large-amplitude or large angle of attack aeroelastic instability studies. The model is suitable, however, for a general study of active control of rotor blade response by systematic variation of the parameters, the purpose for which it is formulated.

Model Development

Basic Equations: Figure 1 shows schematically the blade under consideration. All the velocities are depicted relative to the blade. The mathematical development is somewhat similar to that presented in References 3, 4, and 5, but without the restrictive assumptions inherent in Reference 5. Since the present study includes elastic motions of the blade as well as flapping and feathering, there is no particular advantage to any choice of reference axes for the angular quantities; therefore, the axis of the rotor shaft is selected herein. With regard to standard terminology (Reference 6), the shaft angle is tilted from the vertical through the angle α_s with positive α_s conventionally being taken as rearward. The rest

4

of the terminology corresponds as much as is possible with Reference 6, except that the blade-section pitch angle θ is the angle between the line of zero lift of the blade section and the plane perpendicular to the shaft axis, rather than the plane perpendicular to the axis of no feathering.

The chordwise velocity at the quarter-chord point, in the plane perpendicular to the rotor axis is

$$U_T = \Omega x + V \sin \Omega t + \{ \dot{w} - (Z_{ea} - Z_{xo}) \dot{\theta} + (Z_{\frac{1}{4}}) \dot{\gamma}$$
$$- (Z_{\frac{1}{4}}) (\partial w / \partial x) \Omega \cos \theta \} \sin \theta \qquad (1)$$

where $\cos \alpha_s$ has been replaced by unity in the second term on the right. The term $(Z_{\frac{1}{4}}) (\partial w / \partial x) \Omega \cos \theta$ is derived with reference to Figure 2a. Because of the downward deflection of the blade, the rotation vector (oriented parallel to the Y_O axis) has a component parallel to the elastic axis (that is, in the plane of the blade) of magnitude $\Omega \sin[\tan^{-1}(\partial w \cos \bar{\Phi} / \partial x)]$. Since $\cos \bar{\Phi} = \cos(\theta + \gamma)$, neglecting products of small terms gives $\Omega(\partial w / \partial x) \cos \theta$ for this rotation component. The velocity in the plane perpendicular to the rotor axis, due to this rotation about the elastic axis is $Z_{\frac{1}{4}}$ times this angular velocity. Terms such as this have been variously called gyroscopic or Coriolis effects in the literature.

The velocity at the quarter-chord point parallel to the rotor axis and directed upward is

$$U_P = V\alpha_s - \nu + \{ \dot{w} - (Z_{ea} - Z_{xo}) \dot{\theta} + (Z_{\frac{1}{4}}) \dot{\gamma}$$
$$- (Z_{\frac{1}{4}}) (\partial w / \partial x) \Omega \cos \theta \} \cos \theta + V (\partial w / \partial x) \cos \theta \cos \Omega t \qquad (2)$$

where $\sin \alpha_s$ has been replaced by α_s in the first term on the right. The origin of the term $(Z_{\frac{1}{4}}) (\partial w / \partial x) \Omega \cos \theta$ has been explained previously. The last term on the right is derived with reference to Figure 2b. Because of the blade deflection, the spanwise velocity $V \cos \alpha_s \cos \Omega t$ can be resolved into components parallel to and perpendicular to the blade surface. The component parallel to the span can be neglected (Assumption No. 1) and the perpendicular component can be thought of as having a component along the Y_O axis equal to the spanwise velocity times $\sin [\tan^{-1}(\partial w / \partial x) \cos \bar{\Phi}]$ times $\cos [(\partial w / \partial x) \cos \bar{\Phi}]$, which is equal to the term in question after the small angle assumption is made.

The total velocity U or "relative wind" at a blade cross-section is $\left[U_T^2 + U_P^2 \right]^{\frac{1}{2}}$, and the angle made by U and U_T is the upwash or inflow angle ϕ, as shown in Figure 1. The true angle of attack at a

cross-section is $\alpha_r = \bar{\Phi} + \phi$, which is the angle between the chordline of a symmetrical foil and the relative wind.

Care must be exercised in expressing the lift and drag coefficients for the blade, because of the possibility of reversed flow for $x < V/\Omega$. In developing the lift coefficient relations, only the unstalled regions of angle of attack for forward flight (around $\alpha_r = 0$) or for reverse flow (around $\alpha_r = -\pi$) need to be considered, because of Assumption No. 7. For unstalled forward flight, the lift coefficient is $C_L = C_{LO} \alpha_r$ where C_{LO} is the slope of the lift coefficient versus α_r curve near $\alpha_r = 0$. For unstalled reverse flow, the angle of attack is close to $-\pi$, and the lift coefficient is $-C_{LO}(\alpha_r + \pi)$; the positive lift direction is still upward, which does not coincide with the conventional definition for which positive lift is obtained by rotating the relative wind through $\pi/2$ clockwise. (This slight departure from conventional practice is desirable because it keeps the direction of positive lift upward over the entire span.) When $U_T > 0$, and U_P is small (forward, unstalled flight), the inflow angle $\phi = \tan^{-1} U_P/U_T$ is well approximated by $\phi = U_P/U_T$; when $U_T < 0$ and U_P is small (reverse, unstalled flight), the inflow angle is well approximated by $U_P/U_T + \pi$, i.e., the inflow angle is near π when referred to the positive Z_O direction. Thus, the lift coefficient for a blade section in unstalled forward flight is $C_L = C_{LO}(\theta + \gamma + U_P/U_T)$ and for unstalled reverse flight it is $-C_{LO}(\theta + \gamma + U_P/U_T)$. The lift arising from unsteady pitching, flapping, and bending for the quasi-steady approximation is given by (Reference 1)

$$F_1 = \pi\rho(c/2)^2 \left\{ \ddot{w} - (Z_{ea} - Z_{xo}) \ddot{\theta} + (Z_{\frac{1}{4}}) \ddot{\gamma} \right.$$
$$\left. + U[\dot{\theta} + \dot{\gamma} - \Omega(\partial w/\partial x) \cos\theta] \right\} \tag{3}$$

The small "added-mass" terms can be neglected, so

$$F_1 = \frac{1}{4}\pi\rho c^2 U[\dot{\theta} + \dot{\gamma} - \Omega(\partial x/\partial x)\cos\theta] \tag{4}$$

Combining Equation (4) with the angle-of-attack contributions gives the total lift as

$$F_L = \frac{1}{2}\rho c U^2 C_{LO} \left[\frac{U_T}{|U_T|}\right] (\theta + \gamma + U_P/U_T)$$
$$+ \frac{1}{4}\pi\rho c^2 U[\dot{\theta} + \dot{\gamma} - \Omega(\partial x/\partial x)\cos\theta] \tag{5}$$

The term $\left[U_T/|U_T|\right]$ changes the sign of the angle-of-attack lift contribution in the reversed flow regime, as is required. By using the expressions for U_T and U_P given in Equations (1) and (2), and neglecting products of small terms, the section lift is derived as

6

$$F_L = \tfrac{1}{2} \rho c \, C_{LO} (\Omega x + V \sin \Omega t)^2 \left[\frac{\Omega x + V \sin \Omega t}{|\Omega x + V \sin \Omega t|} \right] (\theta + \gamma)$$

$$- \tfrac{1}{2} \rho c \, C_{LO} (\Omega x + V \sin \Omega t) \left[\nu - V\alpha_s - \dot{w} \cos \theta - V \left(\frac{\partial w}{\partial x} \right) \cos \Omega t \cos \theta \right]$$

$$+ \tfrac{1}{4} \pi \rho c^2 (\Omega x + V \sin \Omega t) \left[\dot{\theta} + \dot{\gamma} - \Omega \left(\frac{\partial w}{\partial x} \right) \cos \theta \right] \tag{6}$$

To simplify the analysis, it has been assumed in Equation (6) that the elastic axis, the cyclic pitch axis, and the quarter-chord point coincide ($Z_{ea} = Z_{xo}$, $Z_{\frac{1}{4}} = 0$); this assumption is not a necessity but does reduce the number of parameters that need to be varied.

The drag force is derived similarly; it is

$$F_D = \tfrac{1}{2} \rho c \, C_{DO} (\Omega x + V \sin \Omega t)^2 \left[\frac{\Omega x + V \sin \Omega t}{|\Omega x + V \sin \Omega t|} \right] (\theta + \gamma)$$

$$- \tfrac{1}{2} \rho c \, C_{DO} (\Omega x + V \sin \Omega t) \left[\nu - V\alpha_s - \dot{w} \cos \theta \right.$$

$$\left. - V \left(\frac{\partial w}{\partial x} \right) \cos \Omega t \cos \theta \right] \tag{7}$$

Here, C_{DO} is a computed slope derived from the drag coefficient versus α_r curve, such that the drag coefficient has approximately the correct values over the operating range of α_r (say, $4°$ to $12°$). This procedure cannot be extended to very small values of α_r because of the non-zero value of drag coefficient for $\alpha_r = 0$; however, it is almost a necessity that the drag force and the lift force have similar functional forms for use with the electromechanical analog, in order to avoid undue complexity. It is also assumed that C_{DO} is the same for the unstalled forward and reverse flow regimes. This latter is a fairly crude assumption, but the drag force is itself small for unstalled flight, so the absolute error in computing the thrust is tolerable. The total section thrust T is equal to $F_L \cos \alpha_r - F_D \sin \alpha_r$. Thus, the final expression for the thrust per unit span at a blade section after neglecting products of small terms is

$$T = \tfrac{1}{2} \rho c \, C_{LO} (\cos \theta - C_{DO}/C_{LO} \sin \theta)(\Omega x + V \sin \Omega t)^2 \times$$

$$\left[\frac{\Omega x + V \sin \Omega t}{|\Omega x + V \sin \Omega t|} \right] (\theta + \gamma) - \tfrac{1}{2} \rho c \, C_{LO} (\cos \theta - C_{DO}/C_{LO} \sin \theta) \times$$

$$(\Omega x + V \sin \Omega t) \left[\nu - V\alpha_s - \dot{w} \cos \theta - V \left(\frac{\partial w}{\partial x} \right) \cos \Omega t \cos \theta \right]$$

$$+ \tfrac{1}{4} \pi \rho c^2 \cos \theta (\Omega x + V \sin \Omega t) \left(\dot{\theta} + \dot{\gamma} - \Omega \left(\frac{\partial w}{\partial x} \right) \cos \theta \right) \tag{8}$$

The aerodynamic torque about the rotation axis caused by the lift and drag on the blade section is

$$Q_x = x(F_L \sin \phi + F_D \cos \phi) \approx (F_L \phi + F_D) x \qquad (9)$$

Thus, after neglecting products of small terms, the section torque turns out to be

$$Q_x = \tfrac{1}{2} \rho c x \, C_{LO} (\Omega x + V \sin \Omega t) \left[\nu - V \alpha_s - \dot{w} \cos \theta \right.$$
$$\left. - V \left(\frac{\partial w}{\partial x} \right) \cos \Omega t \cos \theta \right] \theta$$
$$+ \tfrac{1}{2} \rho c x \, C_{DO} (\Omega x + V \sin \Omega t)^2 \left[\frac{\Omega x + V \sin \Omega t}{|\Omega x + V \sin \Omega t|} \right] (\theta + \gamma) \qquad (10)$$

Integrated Equations: In order to permit the electromechanical analog to be "de-bugged," and to allow values of α_s, θ_c, and ν to be selected with a minimum of trial-and-error, as well as to provide a quick means of verifying that the operational parameters selected are in the range of helicopter practice, the thrust and torque equations are integrated (approximately, for forward flight) over the blade span. The blade is assumed to have a built-in, linearly varying pitch along its span: $\theta = \theta_0 + \theta_0' (x - e_0)$, where θ_0 is the pitch at the blade root, θ_1 is the difference in the pitch between the tip and the root, and $\theta_0' = \theta_1 / \ell$ is the rate of twist. The cyclic pitch is assumed to have a constant amplitude along the entire span, i.e., there is no dynamic, elastic twisting of the blade.

For hovering conditions, the cyclic pitch, θ_c, and V are both zero; for hover, also, the flapping and bending motions do not affect the time-averaged thrust, so Equation (8) can be integrated exactly to give the thrust per blade:

$$T_{avg} = \rho c \, C_{LO} \, R^3 \, \Omega^2 \left\{ \tfrac{1}{6} (\theta_0 - \theta_0' e_0)(1 - E_0^3) + \tfrac{1}{8} \theta_0' R (1 - E_0^4) \right\}$$
$$- \tfrac{1}{4} \rho c \, C_{LO} \, R^2 \, \Omega \, \nu \, (1 - E_0^2) \qquad (11)$$

where $R = \ell + e_0$, $E_0 = e_0 / R$, $\cos \theta$ has been approximated by unity, and the small drag contribution has been neglected. For hover, simple momentum theory (Reference 6) is used to predict the induced velocity:

$$\nu = \sqrt{\frac{b \, T_{avg}}{2 \pi \rho \, R^2}} \qquad (12)$$

where b is the number of blades. The simultaneous solution of Equations (11) and (12) permit ν to be computed for any desired value of thrust. The total torque for the hovering case is, from Equation (10),

$$Q_{total} = \tfrac{1}{2}\rho c\, C_{LO}\, R^4\, \Omega^2 \left\{ (\theta_o - \theta_o' e_o) \left[\frac{\nu}{3\Omega L} + \frac{C_{DO}}{4\,C_{LO}} \right] \right.$$

$$\left. + \theta_o' R \left[\frac{\nu}{4\Omega L} + \frac{C_{DO}}{5\,C_{LO}} \right] \right\} \tag{13}$$

(Equation (13) is used primarily to determine whether the predicted torque has a realistic value for the desired thrust.)

For the _forward_ flight, the blade-section equations cannot be integrated exactly because many of the terms depend on the elastic response of the blade. However, approximate expressions can be formed and used for guidance. These are now developed. The induced velocity and the total thrust, averaged over one blade revolution, are related by the overall momentum equation (Reference 3):

$$\nu^4 + 2V\,\nu^3 \alpha_s + V^2 \nu^2 - \left[\frac{b\, T_{avg}}{2\pi\rho\, R^2} \right]^2 = 0 \tag{14}$$

In this equation, the angle of attack of the rotor disk (tip-plane path) has been replaced by the shaft tilt angle α_s; these angles differ by the cyclic pitch, but since only a first approximation is desired as a starting point, this simplification is acceptable. In fact, in most cases both the first and second terms in Equation (14) are negligibly small. Letting ν_o be the solution when the first two terms are neglected, then

$$\nu_o = \frac{1}{V} \left[\frac{b\, T_{avg}}{2\pi\rho\, R^2} \right] \tag{15}$$

The next approximation to the solution of Equation (14), for small values of α_s, can be derived by an expansion in powers of α_s. The result is

$$\nu = \nu_o - \left[\frac{3\,(\nu_o/V)}{1 + 2\,(\nu_o/V)^2} \right] \alpha_s \tag{16}$$

Equation (16) is one relation between ν and α_s, which are the "unknowns" for a given thrust and forward velocity. Actually $(\partial\nu/\partial\alpha_s)$ is always very small, so it is a good approximation to assume $\nu = \nu_o$. Thus, the approximations in Equation (14) with respect to the rotor angle of attack is not a serious limitation. The true value of the shaft tilt angle α_s must be selected so that Equation (8) gives the correct value for the desired average thrust, when the cyclic pitch θ_c has been simultaneously selected to diminish to zero as nearly as possible the one-per-revolution flapping (elastic and rigid body components) of the blade tip with respect to the

9

shaft axis. In practice, the one-per-revolution thrust component along the shaft axis would probably be minimized. However, both of these procedures result in almost the same cyclic pitch setting, and minimization of the one-per-revolution flapping is more convenient for the electromechanical analog. In order to reduce the amount of trial-and-error in choosing the correct $\nu - \theta_c - \alpha_s$ values with the analog, the one-per-revolution variation in the thrust from Equation (8) is set equal to zero; this, in combination with Equation (15) or (16), gives a set of first approximations. The blade flapping (which should be nearly zero), the elastic motions, and the reversed flow region are neglected in deriving these relations, although, of course, they are retained in the analog development. Integrating Equation (8) along the span, with $w = 0$, neglecting reversed flow, and setting the one-per-revolution time-varying thrust terms equal to zero, the amplitude of the cyclic pitch can be deduced to be equal to

$$\theta_c = \mu \left| \frac{3\left(\frac{\nu \; \cdot \alpha_s}{\Omega L}\right) - 3(\theta_0 - \theta_0' e_0) - \theta_0' R}{1 + 9/4 \; \mu^2} \right| \tag{17}$$

In this equation, $\mu = V/\Omega R$ is the advance ratio. The phase angle, with respect to the downwind position, for the cyclic pitch (when the cyclic pitch is expressed as $\theta_c \cos(\Omega t + \psi_0)$) is also derived in this way:

$$\psi_0 = -\tan^{-1}\left[\frac{6\pi c}{8R \, C_{LO} \, (1 + \frac{3}{4}\mu^2)}\right] \tag{18}$$

Equating the time-average thrust for forward flight to the thrust for hover gives the needed relation between α_s, ν, and V:

$$\alpha_s = \frac{\nu}{V} - \frac{\left[\frac{\nu_H}{V} + \mu(\theta_0 - \theta_0' e_0 + \frac{1}{2}\theta_0' R)\right](1 + 9/4\mu^2) - \frac{1}{2}\mu[3(\theta_0 - \theta_0' e_0) + \theta_0' R]}{1 + 3/4 \; \mu^2} \tag{19}$$

In this equation, ν_H is the induced velocity for hover with the same thrust.

   Equation (15) is used to compute the value of ν used by the analog for forward flight. Equations (17), (18), and (19) are merely used as "first guesses" for θ_c, ψ_0, and α_s; the true values are then determined by trial-and-error on the analog until the desired thrust is obtained and the one-per-revolution variation in the blade tip flapping is minimized.

MODELING CONCEPTS

General

Modeling of the dynamic response of an articulated helicopter rotor blade in forward flight can be accomplished by means of a relatively simple dimensionless analysis which results in the following nondimensional equation,

$$\frac{w}{\ell} = \mathscr{F}\left(\frac{EI}{m\ell^4\Omega^2}, \frac{\rho c\ell}{m}, \frac{c}{\ell}, \frac{e_o}{\ell}, \frac{V}{\Omega R}, \frac{\nu}{\Omega R}, \theta, \frac{F}{m\ell^2\Omega^2}\right) \qquad (20)$$

where all the dimensional variables have been identified in the previous section, except for an arbitrary force F. As previously mentioned, the electromechanical apparatus with which the simulation was to be accomplished was already available for the most part. (The apparatus will be described in more detail in the next section.) Therefore, in order to accomplish a reasonable simulation of a representative prototype aircraft, care had to be exercised in developing the corresponding prototype and model variables. A brief description of this process will now be given.

From Equation (20), it is obvious that dynamic responses for only flapping and bending modes of the rotor blade will be considered. A frequency plot of these modes for the existing model apparatus is shown in Figure 3. Measured frequencies are compared with values predicted from simple beam theory. Note that results are presented up to a maximum frequency to include the third bending mode (13 per rev) only. Above this range, the results become suspect because of force increment resolution. Evidence of this will be discussed later.

Thus, all geometric and structural parameters for the blade were already fixed, and simulation had to be based on a proper selection of blade rotational velocity and air density. By trial and error, a reasonable choice for these parameters was made, and the results are shown in Table 1(a). By the substitution of these results and fixed parameters of the model apparatus into the nondimensional expressions of Equation (20), the corresponding prototype parameters were developed. They are given in Table 1(b), and are considered to be typical for a representative helicopter. A further demonstration of the appropriateness of these prototype values will be given in a later section.

Vortex Impingement

The conditions existing when a vortex shed by a preceding rotor blade impinges on the following blade are described by Scheiman and Ludi

(Reference 7) and Ward (Reference 8). Impingement occurs at the inter-section of the following blade with the path of the preceding blade tip. The trailing vortex of the preceding blade may significantly affect the vibra-tory blade loading of the following blade, producing harmonics of all orders, including significant effects at higher orders.

To simulate the trailing vortex type of impulsive loading phenomena in the model, a time dependent signal, $\nu(t)$, was summed in with the in-duced downwash velocity analog signal in the analog circuit portion of the electromechanical apparatus. This time-dependent signal was a square wave whose duration was initially chosen to simulate prototype vortices of 0.6 meters (2.0 ft) in diameter and 8.5 m/sec (27.8 ft/sec) in ampli-tude. Later, other values of duration and amplitude were used (see Table 4).

Three types of conditions were simulated in terms of the occur-rence of vortex impingement on the following blade. The first condition was a single pulse applied only once, and the second was a repeated "one-per-rev" condition in which $\nu(t)$ was a series of pulses spaced at time intervals equal to one revolution of the blade. The pulses were introduced to the analog circuit controlling the exciter location at the point 88% of the distance from the center of rotation of the blade to the blade tip. The third condition was a "moving pulse" condition in which $\nu(t)$ was a series of pulses, with a given time interval separation, all occurring within one blade revolution. Each pulse in the series was intro-duced to the analog circuit controlling different exciter locations along the blade (see Table 4 for locations). The series of pulses was repeated every revolution of the blade.

The time interval separation of the series of pulses for the moving pulse condition simulated the situation in the prototype where various points along the following blade intersect the path of the preceding blade tip at different times. The time of vortex impingement for any location on the blade depends on the forward flight speed of the aircraft, or advance ratio, μ, the number of blades, b, and the rotational velocity of the blades, Ω.

The relevant equation is:

$$\tan \left[\Omega t_2 - \xi\right] = \tan \Omega t_1 - (V/x) (t_2 - t_1) \tag{21}$$

where $\xi = 2\pi/b$ and b is the number of blades, V is the forward flight velocity, x is the location on the blade, and t_2 and t_1 are the elapsed times of travel of the following and preceding blades, respectively.

12

Figure 4 (obtained by solving the above equation) shows how the point of blade interception by the vortex varies with time for two values of forward flight advance ratio. The $\mu = 0.26$ type movement was not incorporated into the analog circuits because of complexity of implementation. Thus, only monotonic type variation in impulse loading movement was studied. For the $\mu = 0.42$ prototype case, the time interval between pulses for the monotonically moving pulse condition was obtained by locating the corresponding abscissa (time of vortex impingement) for the given ordinates (locations on the blade, i.e., exciter locations) from Figure 4 for the 0.42 advance ratio. This is a series of pulses which moves with time down the blade from the blade tip towards the root, hence, a "moving pulse."

The tip vortex type simulation with monotonic movement is only valid for the prototype, 4-bladed rotor case, at an advanced ratio of 0.42. However, the monotonic variation was also used for the hover case and the $\mu = 0.26$ case. This provided additional dynamic response data that reflects a decrease in number of prototype blades, in the case of $\mu = 0.26$, and also provides an indication of blade response to an impulse, such as an imposed shock front or straight line vortex, moving across the rotor disk in hovering flight.

ELECTROMECHANICAL ANALOG SIMULATION

System Description

Modeling of a helicopter rotor blade experiencing the in-flight environment was accomplished in this study by use of an electromechanical apparatus similar to that described in previous work (References 9 and 10). This apparatus consisted of a pin-free blade rotating at a constant angular velocity and a group of specially-developed analog circuits. Details of the mechanical apparatus, including the blade and rotational device, are described in References 9 and 10. The analog circuit is described below.

The salient features of the blade geometry may be seen in Figure 5. The blade is pinned at the flap hinge a distance e_0 from the center of rotation. The response of the blade at various points (V2 through V10) could be measured from the output of velocity-sensing coils located at those positions. The blade was excited by force coils at the exciter positions shown in the figure. The size and complexity of the analog circuit required to generate current for the force coils limited the number of forcing points which could be used to excite the blade. At many locations two adjacent force coils were coupled in parallel to extend the length over the blade to which the force from one circuit was applied. Where coils were paralleled (F1, F3, F4, F5) the force was assumed to be applied over a distance of 19.1% of the length from the tip of the blade to the center of rotation and around the center point between the exciter locations. For the single coil, F2, the force was applied around point F2, 9.6% of the tip to rotor axis distance.

Generation of the current to drive the force coils at the exciter locations was accomplished with an analog circuit and associated apparatus. As an example, Figure 6 shows a block diagram of the part of this apparatus used to generate the force at location F5 (similar circuits were used to generate the forces at the other excitation points). Input to the analog circuit was the blade response at V8 and V10. These responses were summed and divided to obtain a velocity signal equal to their amplitude average at any time, $\dot{w}_5$. This velocity signal was assumed to be equivalent to the velocity response of the beam at midpoint for the excitation points of F5, x_5.[*] The difference between the blade response signal from V10 and V8 was integrated with time to obtain a signal propostional to the instantaneous difference in displacement of the blade, w_5, at locations V10 and V8. Thus, a signal $(\partial w / \partial x)_5$, the displacement slope of the

---

[*]Note that the V9 signal could also have been used for this response; however, the use of V8 and V10 was required anyway in developing the slope of displacement in the forcing increment.

14

blade at x_5, could be generated. Constants input to the analog circuit were: d.c. voltages simulating the time invariant value of blade pitch, θ_5, at blade increment 5; the induced downwash velocity, ν_o; the product of the forward flight speed and the shaft tilt angle, $V\alpha_s$; and the product of the rotation speed and x_5, Ωx_5. A one-per-rev generator attached to the mechanical simulator rotor axis generated a signal, $\sin \Omega t$, input to the analog circuit, and a phase shifter was used to obtain $\sin(\Omega t + \psi_o)$ as another input.

The details of the many analog computations are shown only in rough form in the block diagram. The last element of the circuit was a power amplifier (voltage-to-current converter) used to convert the signal, F5 into a current to drive the force coils. Referring back to Equations (6) and (7), the equation for F5 the output of the analog circuit, in terms of circuit input signals is:[*]

$$F5 = -0.25\pi \, \Delta x_5 \rho c^2 \cos \theta_5 \, (\Omega x_5 + V \sin \Omega t) \left[\dot{\theta}_5 - \Omega \left(\frac{\partial w}{\partial x} \right) \cos \theta_5 \right]$$

$$- 0.5 \, \Delta x_5 \rho c \, C_{LO} \left(\cos \theta_5 - \frac{C_{DO}}{C_{LO}} \sin \theta_5 \right) (\Omega x_5 + V \sin \Omega t)^2 \frac{U_T}{|U_T|} \theta_5$$

$$+ 0.5 \, \Delta x_5 \rho c \, C_{LO} \left(\cos \theta_5 - \frac{C_{DO}}{C_{LO}} \sin \theta_5 \right) (\Omega x_5 + V \sin \Omega t) \times$$

$$\left[\nu_o - V\alpha_s + \nu(t) - \dot{w}_5 \cos \theta_5 - V \left(\frac{\partial w}{\partial x} \right)_5 \cos \Omega t \cos \theta_5 \right] \qquad (22)$$

where

$$\Delta x_5 = 19.1\% \, (e_o + \ell)$$

$$x_5 = 88\% \, (e_o + \ell)$$

$$\dot{w}_5 = (V10 + V8)/2$$

$$(\partial w / \partial x)_5 = \int (V10 - V8)/\Delta x_5 \, dt$$

$$\theta_5 = \theta_o + \theta_o' (x_x - e_o)$$

$$\theta_5(t) = \theta_5 + \theta_c \sin(\Omega t + \psi_o)$$

$$\dot{\theta}_5 = \theta_c \cos(\Omega t + \psi_o)$$

and where θ_c and ψ_o are cyclic pitch amplitude and phase, respectively. θ_o' is the blade twist per unit length; ℓ is the blade length; ρ is the air density; c is the blade chord; and C_{DO} and C_{LO} are the slopes of the drag and lift coefficients versus angle of attack for a blade shape NACA 0012.

---

[*] Note that in Equation (22), the algebraic sign has been set to minus the aerodynamic force. This is done in the analog in order to make a positive force correspond to a positive w, to conform with ordinary beam theory.

Values for the fixed parameters for this study: ℓ, c, e_o, ρ, m, θ_1, b, C_{LO}, and C_{DO} are given in Table 1. Values for the parameters varied during the study: θ_o, V, α_s, θ_c, ψ_o, and ν_o are given in Table 2. The parameter $\nu(t)$ was generated by a pulse generator as described in the section on Vortex Impingement.

Procedures for Initial Conditions

The electromechanical model was run for a series of tests to simulate in-flight conditions of a helicopter rotor blade. Those conditions for various advance ratios, μ, in which $\nu(t)$ was zero (no vortex impingement) and no external damping, δ, was applied to the blade, are referred to as the "initial conditions." A series of these initial conditions, one for each of three μ's chosen, was run for each of three chosen values of collective pitch, θ_o (see Table 2 for values).

The procedure for obtaining the initial conditions at any μ for a given θ_o was as follows. The constants θ for each location x were adjusted everywhere in the analog circuits to the appropriate value.

$$\theta = \theta_o + \theta_o' (x - e_o)$$

ν_o was adjusted in the circuits to the value determined from Equations (12) or (15). The thrust per blade, T_{avg}, was measured for $\mu = 0.0$ (V = 0.0), hover condition, by multiplying the time-averaged sum of the analog circuit signal outputs by the appropriate conversion constant. This measured thrust (see Table 2) was checked against the theoretical value determined from Equation (11). A close correspondence indicated all systems were functioning normally. In addition to this check, the quantity $\Omega x^2 \theta \nu_o \Delta x$ was measured from each of the five forcing circuits and summed to obtain an approximate torque per blade at hover.

$$Q = \sum_{i=1}^{5} \frac{1}{2} \rho c \ C_{LO} \ (\Omega x_i^2 \ \theta \ \nu_o) \ \Delta x_i$$

Note from Equation (13), that the drag terms were omitted in this measurement. This rather crude approximation was utilized because of a lack of sufficient analog components. As a result, the measurement was made only for hover conditions. The measured value (see Table 2) was checked against the theoretical value at hover obtained from Equation (13). These checks assured that the behavior of the electromechanical model closely corresponded to the theoretical or math model, and that all systems of the electromechanical model were operating properly.

16

Initial conditions for the two forward flight configurations were obtained by adjusting the amplitude of $V \sin \Omega t$ in the analog circuit to the desired value, then adjusting the d.c. term $-V\alpha_s + \nu_0$ to a level which brought T_{avg} back to the same value obtained at hover. While operating the model, a response output near the tip of the blade, V9 (see Figure 5 for location), was analyzed simultaneously with an oscilloscope and a spectrum analyzer. Components θ_c, the cyclic pitch amplitude, and ψ_0, the cyclic pitch phase, were adjusted in the circuit until the one-per-rev component of V9 was minimized, while at the same time trimming the term $\nu_0 - V\alpha_s$ to maintain the desired thrust. It will be seen later that this procedure resulted in realistic values of the operating conditions. When these initial conditions were obtained, scope trace photographs were taken of the velocity response V7 and V9 and the total a.c. component of the thrust I_t (see Figure 7). The latter component is the vector sum of the fluctuating part of the thrust at all blade increments. Note that in the expanded scale of Figure 7a, some one-per-rev component of V7 and V9 remains after minimization for $V = 0$, although no external impulses were being applied. This response results from small amounts of beam unbalance in the mechanical rotor. These records, along with the spectral plots of V9 to be described later, were used as a reference for the initial conditions and assured that we could return to those conditions at any time and know the model was functioning consistently.

With the model running under initial conditions, the values of θ_c, ψ_0, T_{avg}, and $-V\alpha_s + \nu_0$ could be measured. The value for ν_0 at the forward flight speeds was obtained from Equation (15) and the measured T_{avg}. The value for α_s could then be determined from the measurement for $\nu_0 - V\alpha_s$. All measured values for operation of the model in initial conditions are given in Table 2. Plots of thrust coefficient, C_T/σ, as a function of shaft tilt angle for prototype rotor blades operating at our values for μ and θ_0 were obtained from W. H. Tanner's work on rotary wing performance (Reference 11). Since the charts and graphs in Reference 11 are referred to the axis of no feathering, it was necessary to account for the cyclic pitch in correlating these values to the quantities used in the present study, which are referred to the shaft axis. Essentially, this amounted to adding the cyclic pitch to the rotor angle of attack (α_c, in the terminology of Reference 11) to obtain the shaft tilt angle shown in Figure 8. From the measured thrust, a "measured" thrust coefficient could be calculated for any initial condition using the equation:

$$\frac{C_T}{\sigma} = \frac{T_{avg}}{\rho c b R^3 \Omega^2}$$

Values for C_T/σ obtained from measured thrust and the associated measured α_s for any given initial condition are compared to the results of Reference 11 in the plot of Figure 8. The reasonable comparison of the

measured and theoretical values assured us that our model simulated a realistic prototype rotor blade operating under realistic conditions.

Procedures for Test Runs

Having established initial conditions as described in the previous section, the model was run for a variety of test conditions in which a signal simulating vortex impingement was summed into the analog circuit. Furthermore, the effect of external damping on the blade response under these conditions was investigated by feeding back the negative velocity response signal from certain points of the circuit to their corresponding exciter points. Thus, in effect, an equivalent viscous type damper resulted.

It was pointed out in a previous section that one would expect the electromechanical simulation to become invalid at some intermediate frequency because of the finite size of the forcing distribution increment. That is, for shorter bending wave lengths, both the simulated aerodynamic feedback and simulated damping feedback concepts break down. Some preliminary experimentation was performed to determine the useful upper frequency limit for the apparatus. It was found that damping feedback had a strong tendency to amplify response above 10-per-rev, rather than provide positive damping. This result seemed plausible in view of the fact that the wavelength of the third bending mode is comparable to the force distribution increment (see Figures 3 and 5). As a result, all responses fed back in the analog were low-pass filtered above 16-per-rev to reduce this tendency. It is estimated that only results below 10-per-rev are valid, however. All results presented herein should be understood to include this restriction.

Preliminary experimentation was also conducted to determine the general type of responses that occurred for several different type of excitation pulses considered for demonstrating the effectiveness of the damping feedback. In addition to those described in the results to follow, a single pulse was also considered. However, for those pulse shapes utilized, the responses did not extend in time beyond a single blade revolution, so that the results can be deduced from those of a pulse repeated at one-per-rev, and data on the single pulse was not acquired.

Table 3 gives the matrix of test conditions investigated. Table 4 explains in detail what the simulation function $\nu(t)$ looked like in every instance. These different functions are coded in the matrix itself under a single "p" number. Three levels of feedback were used. Values for the damping force per unit velocity, δ, were 0.0, 1.96 × 10³ N/m/sec, and 3.92 × 10³ N/m/sec, and are coded in Table 4 as $\delta = 0$, 1, and 2, respectively.

18

Two different locations for damping feedback were simulated. Outboard damping feedback was accomplished by amplifying the V9 velocity signal to a desired level and feeding the result back into force exciter F5. Inboard damping feedback was accomplished by amplifying the V7 velocity signal to a desired level and feeding the result back into force exciter F4.

The amplitudes and time widths of the pulses described in Table 4 were arbitrarily chosen to represent something like the inflow velocity disturbance caused by the impingement of a vortex shed from a preceding blade. The amplitudes were comparable to the steady inflow velocity v_0, and widths were of the order of 0.6 meter or less in space.

SIMULATION RESULTS

Preliminary Comments

Results for a given collective pitch θ_O can conveniently be separated into three broad categories: steady state flight, the one-per-rev pulse condition, and the moving pulse condition. These categories relate to the type of function $v(t)$ applied as defined in Table 4, and the results for each category will be presented separately below. Some explanation of results which tend to verify the validity of the simulation will also be presented. Further discussion related to results from the use of damping feedback will be presented in a following section. In all cases, the results are presented in terms of prototype parameters for greatest utility, although the measurements were, of course, performed on the model.

Generally, the data is presented in several forms. Oscilloscope photographs of response time histories are given for key examples to show blade motion at several locations. Most of the data were acquired in the form of root mean square response amplitude and spectral decomposition of the response at V9. Recall again that V9 is the output of the second velocity transducer from the blade tip (see Figure 5). In some cases, oscilloscope time histories were also obtained for responses at V7, and are also presented. It would, of course, have been desirable to acquire data at all response points along the blade. However, this would have resulted in a further increase in an already large volume of data. Thus, it was considered feasible to form conclusions about blade response behavior from V9 results alone.

All details of RMS and spectral response data are presented in the several tables of Appendix A. However, a substantial number of sample plots of these data for $\theta_O = 12°$ only, will follow below in order to provide a more convenient basis for discussion and forming conclusions. Root mean square amplitude data are presented in two forms: "as measured" (Table A-1), and "corrected" (Table A-2), narrow band results which are valid through 10-per-rev. These results were obtained by forming the combined RMS values from the first 10 components of the spectral data given in Appendix A. As described in previous sections, this range of frequency was considered valid for the analog simulation system. In addition, the corrected RMS response values include an accounting for certain crosstalk noise that appeared on V9 for those conditions where a pulse was applied (details to be given later). All RMS amplitude response plots to follow are based on such narrow band results, and those for pulse applied conditions are based on corrected narrow band results.

Finally, spectral data were acquired up to 16-per-rev, and in some cases beyond this. Results are generally presented up to 16-per-rev, since this range was convenient for analysis purposes. However, those components above 10-per-rev should be considered invalid, and studied only for indication of how rapidly the simulation breaks down as frequencies increase.

Steady State Flight

Under steady state flight, no external pulse is applied to the blade, i.e., $\nu(t) = 0$. For this condition, the oscilloscope photographs of response time histories have already been shown in Figure 7. It is interesting to note that the response at both V7 and V9 is largely at 2-per-rev, and at $\mu = 0.42$ the response at 2-per-rev is nearly equal in amplitude for both positions. By referring to Figures 3 and 5, this response can be concluded to occur principally from motion in the flapping and first bending modes, and the phasing must be such that the blade tip motion in each mode is out of phase, and the flapping response must be larger than than of the bending.

Further data are shown in Figures 9 through 12. Figure 9a shows an example plot of the narrow band RMS amplitude response at V9 as a function of advance ratio μ, for fixed collective pitch $\theta_0 = 12^\circ$, and for outboard damping feedback set at several different levels. A complete set of these data for all flight conditions is presented in Table A-1. Further similar RMS response data are presented in Figure 9b for inboard damping. From these data it was decided that the effect of damping feedback at the inboard location was negligible. As a result, hereafter damping feedback was limited to the outboard location only.

Figures 10 through 12 show example plots of the spectral response for V9 and steady state flight conditions. Similar data are tabulated in Table A-3 for all values of collective pitch. From these figures it can be seen that for the steady state conditions defined, the major components of response in the blade occur at the first four harmonics of blade rotation, i.e., at 1, 2, 3, and 4-per-rev. From Figure 3 this can be seen to be response principally in the flapping and first bending mode. The only small to negligible responses at 6 and 7-per rev, and near 11 and 12-per-rev, indicate that very little motion in the second and third bending modes respectively, is present in the response at V9. By inspection of Figure 5, it can be seen that V9 is located near a node for both the higher modes. Thus, motion in these modes is probably present in the overall blade response, but only a relatively small amount of it can be detected at V9.

Even without the previously-described method of nulling the one-per-rev component for initial steady state conditions, one might again

wonder why vibration at any frequency is present for the hover condition shown in Figure 10. As was previously explained, some vibration is excited by residual unbalance in the mechanical rotor system. This vibration is given by the results in Figure 10a. The amplitude of the component at one-per-rev would be far greater in Figures 11 and 12, which correspond to forward flight speed conditions, had the trimming not been used in the initial condition procedures. Note also that for forward flight speeds, the one-per-rev component could not be completely eliminated because the phase of the unbalance excitation does not coincide with that from forward flight excitation.

Repeated Pulse

For this series of tests, $\nu(t)$ was implemented as described in Table 4 for $p = 1$ or 3. Essentially, these tests simulated a vortex of two different diameters and velocity amplitudes impinging at the F5 exciter location once every revolution of the blade. Figures 13a and 13b show time histories of the blade response at V7 and V9 for hover and for the higher forward speed, where no external damping has been included. The applied inflow velocity pulse in this case has an amplitude of 8.47 m/sec and a diameter of 0.6 m. The affect of the inflow velocity pulse on the fluctuating component of the total blade thrust, I_t, can be obtained from the lower trace in each figure. Note, however, that inadvertently the pulse was lost off the bottom of the photograph in Figure 13b. For this case it would appear as a pulse downward with the same amplitude as in the bottom trace of Figure 13a. The upper trace in all these figures represents only a timing reference signal for marking one-per-rev, at $\Omega t = 90°$.

Figures 13a and 13b should be compared directly with Figures 7a and 7c. Note again, however, that a different scale was used in Figure 7a. It can be seen that the effect of the pulse is to excite principally responses at several times the blade rotation, with smaller changes to the response in the range of one-per-rev. It is also apparent that a pronounced high frequency downward and upward spike occurs at V9 during the application of the pulse, followed by a ringing of the blade at frequencies of 3-per-rev and above. Only the ringing type response is apparent in the V7 signal. A careful scrutiny of the pulse part of the response at V9 led to the conclusion that this part of the signal is error due to cross-talk between the velocity response transducer at V9 and the two force exciters on either side of it which made up F5 (see Figure 5). Note that this essentially added noise did not extend all the way to V7. It was determined that the cross-talk could not be eliminated without significant changes in the apparatus. A numerical correction procedure was developed to eliminate approximately the effects of the cross-talk from the V9 RMS response data. First, a spectral analysis was performed for signals similar to V9 and I_t in Figure 13a, which approximated the presence of the pulse only. This spectral analysis had

22

components of uniform amplitude at all integer-per-rev frequencies in the range of 16-per-rev and even higher. This uniform amplitude was considered a noise level which was found to vary slightly with the type of pulse applied. Corrected narrow band RMS data were formed by subtracting out the effects of the noise from each component. The difference in uncorrected and corrected RMS response values can be obtained by comparing corresponding data from Tables A-1 and A-2. The appropriate noise levels are noted on all spectral plots for conditions in which a pulse was applied.

In retrospect, the above problem could also have been avoided by analyzing signals at V7 instead of those at V9. However, none of the final conclusions from the study would have been altered.

Root mean square amplitude response for the $p = 1$ repeated pulse condition and three levels of outboard damping appear in Figure 14, and corresponding spectral plots appear in Figures 15 through 17. The RMS data indicate that external damping decreases the response for the range through 10-per-rev. The spectral plots of Figures 15 and 17 also confirm the results presented in Figures 13a and 13b. That is, for a given level of external damping or suppression, the effect of the pulse is to excite responses at frequencies of 3-per-rev and above, with smaller changes to the 1 to 2-per-rev components.

Additional RMS amplitude and spectral data appear in Figures 18 and 19 through 21, respectively for the $p = 3$ pulse condition. Basically, the same conclusions stated above apply also to these results with one exception. It is apparent for this case that the higher feedback suppression level tends to increase the RMS level rather than decrease it at the lower speeds. From Figures 19 through 21, and Figure 3, it can be seen that this behavior is associated with a decrease in damping of the third bending mode near 12-per-rev. Apparently the phasing of the response of this mode is such that the damping adds energy rather than removes it. It should also be noted from Figure 5, however, that the F5 exciter, at which the external damping is applied, is located near a node for this mode. Thus, this result is in question, and probably is invalid because of the size of the finite blade increment as already described. In any event, this mode occurs above the 10-per-rev range, although its effects in this case are apparently being felt down into this frequency range.

Moving Pulse

For this series of tests, $\nu(t)$ had the characteristics described in Table 4 for $p = 2$ and 4. These tests were performed to measure the blade response for an impulse loading which intercepts a blade at a series of points traveling from the blade tip toward its root. The response time histories for V7 and V9 for hover and high forward speed with the $p = 2$

pulse condition applied are shown in Figure 22. In addition to this condition being formed by a repeated pulse, the polarity of the inflow impulse was also reversed. This can be seen from the upward protrusion of the pulses shown in the lower traces of Figures 22a and 22b, as compared with the corresponding downward protrusion of the pulse in Figure 13, for the $p = 1$ single repeated pulse. Note from the I_t trace that the inboard-most pulse was too weak to appear.

It is apparent from these figures that a similar high frequency response is excited by this pulse condition when compared to the responses in Figures 13a and 13b. However, the responses at 1-2-per-rev also appear to be influenced more, as might be expected. Further, the responses of the moving pulse appear to carry over into the next blade revolution, rather than damp out in a single revolution, as appeared to be the case in Figure 13 for the $p = 1$ pulse.

The same comments made in the previous section about the cross coupling spike response also apply for this case. Therefore, a similar numerical correction was developed to eliminate approximately the effects of the cross-talk noise from the RMS response results. All plotted data are again based on corrected values.

Root mean square amplitude of the response at V9 is shown in Figure 23 for the $p = 2$ condition. The results here are basically similar to those shown in Figure 14 for the $p = 1$ condition. However, the levels at hover are higher in the moving pulse case. These results are confirmed by the spectral plots which appear in Figures 24 through 26. It is apparent that the increased vibration response at hover occurs in the 1-3-per-rev region. Thus, these data support the similar conclusion formed from Figure 22, that the moving pulse has a greater influence on the lower frequency response than the single repeated pulse.

A corresponding set of plotted data for RMS response and spectral decomposition are presented in Figures 27 through 30 for the $p = 4$ condition. Careful study of these data reveal a behavior similar to that for the $p = 3$ single repeated pulse condition shown in Figures 18 through 21. However, in going from $p = 2$ to $p = 3$, again the responses at lower speeds (including hover) appear to be influenced the most. This change in response is also concentrated principally in the 1-3-per-rev range.

A response simulation for the $p = 4$ case could not be achieved for a collective pitch of $\theta_0 = 11°$ (see Table A-7 in the Appendix). For this case, the system went unstable at the high forward speed ($\mu = 0.42$). As a result, data for this case were taken for the $p = 5$ condition defined in Table 3. The system remained stable for the latter case. It should be emphasized that this instability most likely resulted from the improper simulation above 10-per-rev, rather than any response in the valid frequency range.

DISCUSSION

The preceding sections have already included a substantial amount of discussion of results presented. However, that discussion has been aimed principally at pointing out aspects of the data which tend to verify the validity of the simulation, and to show that various forms of results obtained were consistent. The purpose of this section is to emphasize the utility of the results presented in this report for consideration in the potential design of active feedback suppression systems in actual rotary wing aircraft. Of necessity, some of the discussion will expand upon that already presented.

Generally, the results show that the use of an active response suppression device can be quite effective in reducing the overall response of the vibrating rotor blade. However, the location of the device obviously has a strong influence on those modes that can be suppressed. It is apparent that the device must be located near the tip of the blade to be the most effective. This result could have been deduced intuitively; however, one might not have realized how dramatic the effect was in moving from $x = 4.42$ meters out to $x = 5.6$ meters, as shown in Figure 9. It would even be more desirable to select a position even nearer the blade tip, which would correspond to an antinode position for most of the lower modes. Note that the F5 position in the present study nearly coincides with nodes for both the second and third bending modes. As a result, little suppression of these modes could be accomplished.

After a careful study of all of the data near the end of the program, it became apparent that the early conclusion about the overall ineffectiveness of inboard damping probably was premature. The outboard damping was effective in suppressing the 1-3-per-rev flight loads response which was primarily blade flapping and first bending. The outboard feedback was active in both of these modes. However, the situation appeared to be reversed for the impulse suppression. The outboard feedback was not active in the second and third bending modes as a result of the feedback location being at the node points of these modes. Therefore, the outboard feedback location tended to be ineffective in suppressing the higher frequency blade response associated with impulse loading. Unfortunately, the results are inconclusive regarding inboard feedback location suppression of impulse response. However, the inboard location had higher participation in the second and third modes and, therefore, could be expected to be more effective in impulse response suppression.

In most of the spectral data presented, it appears that the 1 and 3-per-rev components were significantly reduced by the outboard damping,

but the 2-per-rev component was essentially unaltered for most cases. The reason for this is not clear. It has been mentioned that the 2-per-rev component must be comprised principally of the flapping and first bending modes. However, these occur very nearly at 1-per-rev and 3-per-rev, respectively. Thus, if these components are reduced by damping, it seems reasonable that the 2-per-rev component should correspondingly reduce. It is plausible that the addition of external damping causes a shift in the phasing of the responses of the two modes such that the vector sum of the two still is affected relatively little, although the individual amplitudes are reduced. Interaction with the effects of the cyclic pitch may also be the source of this behavior. In the present case, cyclic pitch was adjusted for a minimum 1-per-rev initial condition and then external damping was applied. Further adjustment of cyclic pitch thereafter may have reduced the 2-per-rev component, had this been attempted. In any event, this result can be most significant in design.

Another lesson must be learned from the effects of the location of the suppression device on damping characteristics. Considerable care had to be exercised with the model rotor blade to filter out higher mode response above 16-per-rev to avoid instability in those modes. This difficulty was caused by the use of a finite increment in representing the aerodynamic and damping force on the blade. Thus, in practice, care will have to be taken to assure that the response sensor and reaction force applicator are located very near each other in order to avoid a similar instability from occurring in a prototype system.

In this present study, the diameter of a vortex was assumed to be about 0.25 meter or smaller. It is apparent from the results that such a narrow repeated rapping of the rotor caused principally high frequency response, although the moving pulse did have a relatively significant effect on responses below 4-per-rev. A careful investigation should be pursued to determine whether larger diameter vortices are realistic. If they are, it is apparent that considerably greater lower frequency responses will be excited by such larger diameter (wider pulse vortices). At the same time, an investigation of realistic vortex amplitude is also warranted, since this parameter has a significant influence on the response results.

The results of the present study can be used to provide some idea of design parameters for external active modal suppression. The RMS results can be used directly to arrive at a damping effectiveness coefficient in terms of percent vibration reduction per unit of damping force (N/m/sec) applied. From the several RMS plots it is obvious that this coefficient would vary with μ as well as the type of pulse excitation considered. However, an average value would be of the order of $30/1.96 \times 10^3$ percent per N/m/sec, or about 0.015% per N/m/sec applied.

Various limitations of the present apparatus have been pointed out in the discussion throughout this report. However, it has still provided useful information directly applicable to design of actual active modal suppression devices for helicopter rotor blades. Having the benefit of this first experience in studying this problem, a variety of further studies suggest themselves. Obviously the significance of higher frequency response and possible instability can be investigated by using more of the total of nine force increments available with the mechanical blade. Unfortunately, this dictates the use of a more elaborate analog computer system. The possibility of using more sophisticated aerodynamic theory can be considered. Considerably more data could be taken and analyzed from other blade response positions, even with the present facility. It is particularly obvious now that more work with inboard damping and impulsive loading conditions would yield further useful results. The matter of avoiding cross-talk between force and response channels could be better effected. With a little more effort, a vortex impingement pattern appropriate for the prototype rotor at $\mu = 0.26$ could be achieved. A more elaborate analog setup would also have allowed a more accurate confirmation of total torque as well as total thrust. Even so, it is felt that the effort has allowed a preliminary, but significant, demonstration of the effectiveness of active feedback suppression by means of a rather unique technique.

TABLE 1(a). MODEL PARAMETERS

$$\Omega_m/\Omega_p = 2.5 \qquad \rho_m/\rho_p = 1.428$$

$$V_m/V_p = 0.216 \qquad F_m/F_p = 4.98 \times 10^{-4}$$

Bending Number

$$\frac{EI}{m\ell^4\Omega^2} = 0.00923$$

Flapping Inertia

$$\frac{3\pi\rho c\ell}{m} = 2.73$$

TABLE 1(b). HELICOPTER FIXED PARAMETERS

	Prototype	Model
Blade Length, ℓ	6.01m (19.7 ft)	0.519m (1.70 ft)
Number of Blades, b	4	4
Flap Hinge Eccentricity, e_o	0.354m (1.16 ft)	3.06×10^{-2} m (0.100 ft)
Blade Chord, c	0.533m (1.75 ft)	4.61×10^{-2} m (0.151 ft)
Air Density, ρ	1.23 kg/m^3 (1.15×10^{-7} lb-sec^2/in^4)	1.75 kg/m^3 (1.640×10^{-7} lb-sec^2/in^4)
Mass per Unit Length, m	13.6 kg/m (9 lb/ft)	0.145 kg/m (9.60×10^{-2} lb/ft)
Blade Stiffness, EI	1.58×10^5 N-m^2 (5.5×10^7 lb$_f$-in^2)	0.588 N-m^2 (2.05 lb$_f$-in^2)
Rotational Speed, Ω	300 RPM	750 RPM
Max. Blade Twist, θ_1	$-8°$	$-8°$
Slope of Drag Coefficient, C_{DO} (Blade NACA 0012)	.092/rad.	0.092/rad
Blade Tip Speed, $(e_o+\ell)\Omega$	200 m/sec (655 ft/sec)	43.2 m/sec (141 ft/sec)
Slope of Lift Coefficient, C_{LO} (Blade NACA 0012)	6.13/rad.	6.13/rad

TABLE 2. MEASURED PROTOTYPE HELICOPTER VARIABLE PARAMETERS

Collective Pitch, θ_o, deg (at blade root)	10			11			12		
Advance Ratio, μ	0	0.26	0.42	0	0.26	0.42	0	0.26	0.42
Forward Speed, V, m/sec (ft/sec)	0 (0)	52.4 (172)	84.1 (276)	0 (0)	52.4 (172)	84.1 (276)	0 (0)	52.4 (172)	84.1 (276)
Shaft Tilt Angle, α_s, deg	0	-6.10	-3.72	0	-6.75	-3.76	0	-6.36	-3.66
Cyclic Pitch Amplitude, θ_c, deg	0	2.80	2.56	0	3.57	3.33	0	4.43	4.02
Cyclic Pitch Phase, ψ_o, deg	0	3.95	4.65	0	3.25	3.25	0	4.00	4.00
Inflow Velocity, ν_o, m/sec (ft/sec)	6.75 (22.15)	0.875 (2.87)	0.545 (1.79)	7.97 (26.16)	1.23 (4.04)	1.08 (3.56)	9.13 (29.95)	2.31 (7.57)	1.44 (4.72)
Thrust Per Blade, T_B, N x 10^{-3} (lb_f)	4.09 (920)	4.09 (920)	4.09 (920)	5.19 (1166)	5.19 (1166)	5.19 (1166)	6.62 (1488)	6.62 (1488)	6.62 (1488)
Torque Per Blade, Q, N-m x 10^{-3} (ft-lb_f x 10^{-3})	2.44 (1.80)	--	--	3.62 (2.67)	--	--	4.92 (3.63)	--	--

TABLE 3.   MATRIX OF TEST CONDITIONS

θ_o deg	μ	p^*	δ^*	θ_o deg	μ	p	δ	θ_o deg	μ	p	δ
12	0	0	0, 1, 2	11	0	0	0, 1, 2	10	0	0	0, 1, 2
		1	"			1	"			1	"
		2	"			2	"			2	"
		3	"			3	"			3	"
		4	"			4	"			4	"
	0.26	0	"		0.26	0	"		0.26	0	"
		1	"			1	"			1	"
		2	"			2	"			2	"
		3	"			3	"			3	"
		4	"			4	"			4	"
	0.42	0	"		0.42	0	"		0.42	0	"
		1	"			1	"			1	"
		2	"			2	"			2	"
		3	"			3	"			3	"
		4	"			4	"			5	"

* See Key to Test Matrix on next page.

TABLE 4. CHARACTERISTICS OF APPLIED PULSES AND GUST SUPPRESSION

Applied Pulse $\nu(t)$			
Pulse Condition p	Pulse Amplitude m/sec (ft/sec)	Pulse Width millisec	Point and Rate of Application
0	0	0	No pulse applied
1	8.47 (27.8)	3.0	$R - e_o = 0.88$ (at F5), and 1-per-rev*
2	8.47 (27.8)	3.0	$R - e_o = 0.88, 0.69, 0.50, 0.36, 0.21$† (at F5, F4, F3, F2, F1) & 1 each per rev
3	25.4 (83.4)	1.0	$R - e_o = 0.88$ (at F5), and 1-per-rev
4	25.4 (83.4)	1.0	$R - e_o = 0.88, 0.69, 0.50, 0.36, 0.21$ (at F5, F4, F3, F2, F1) & 1 each per rev
5	16.9 (55.6)	1.5	$R - e_o = 0.88, 0.69, 0.50, 0.36, 0.21$ (at F5, F4, F3, F2, F1) & 1 each per rev

Gust Suppression Feedback	
Damping Condition δ	Damping Constant N/m/sec
0	0
1	1.96×10^3
2	3.92×10^3

* Since the response of the blade is unaffected by the applied pulse for times longer than one blade revolution (see Figure 13 for example), a single applied pulse produces the same response in the blade as appears for one revolution of the p = 1 condition.

† See Figure 4 for source of these data.
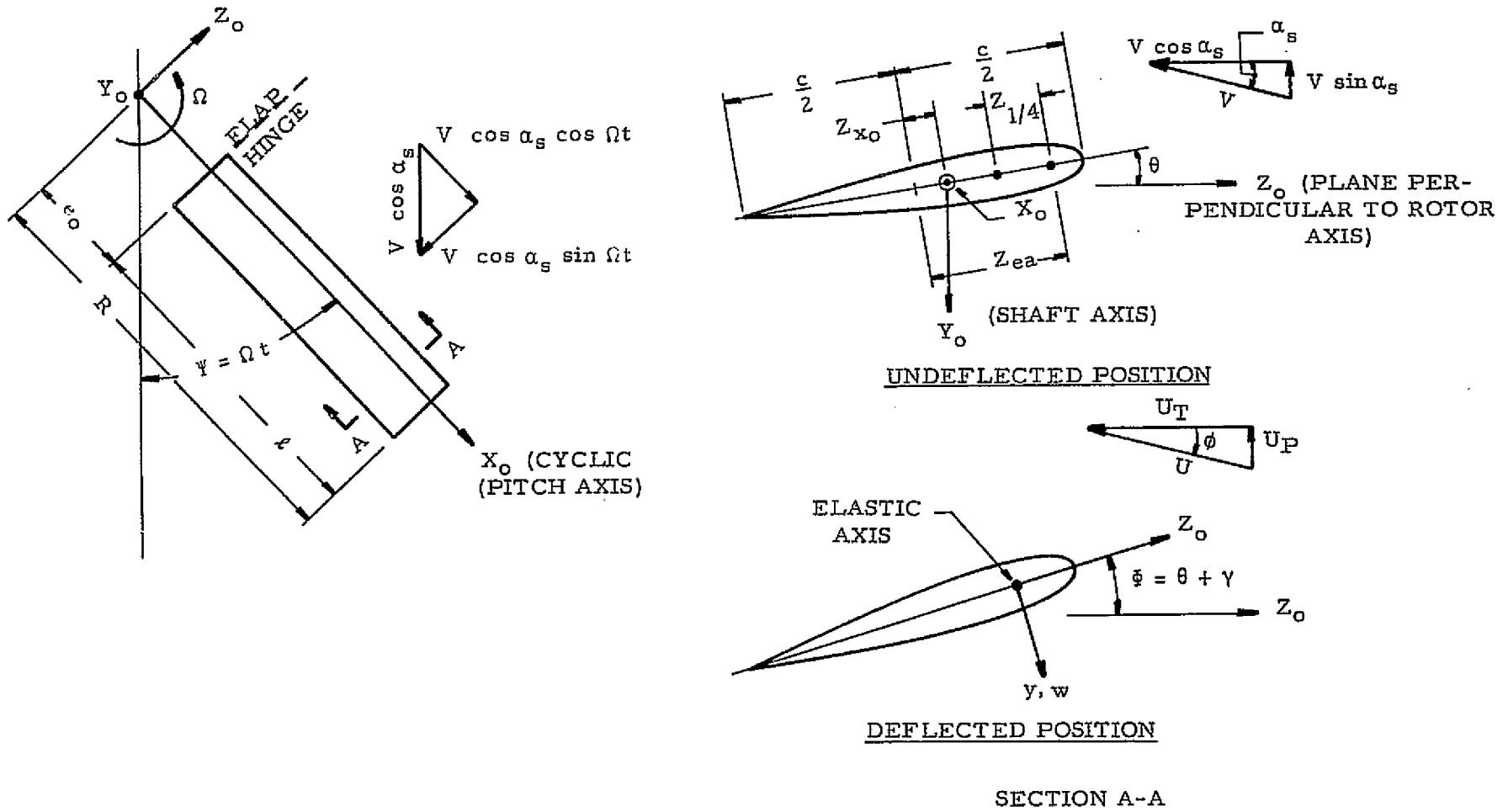
Figure 1. Velocity Relationships and Schematic of Single Rotor Blade

$$\text{ANGLE} = \tan^{-1}\left(\frac{\partial w}{\partial x}\ \cos\ \Phi\right)$$

ELASTIC AXIS
(Deflections greatly magnified)

NOTE: dw cos Φ = component of dw
along Y_0 axis
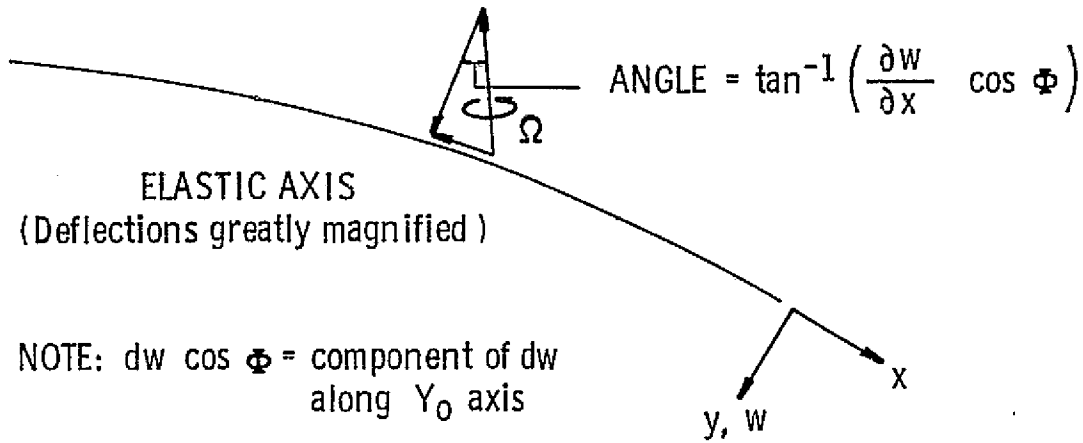
(a) Rotation component in place of blade

ELASTIC AXIS

$V\ \cos\ \alpha_s\ \cos\ \Omega t$

$$\text{ANGLE} = \tan^{-1}\left(\frac{\partial w}{\partial x}\ \cos\ \Phi\right)$$
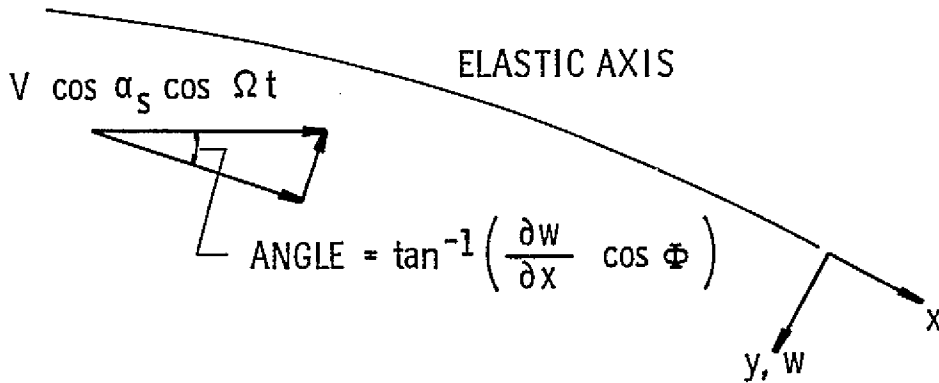
(b) Span-wise velocity component perpendicular to blade

Figure 2. Relationships between angular velocity or span-wise velocity
and the blade deflections
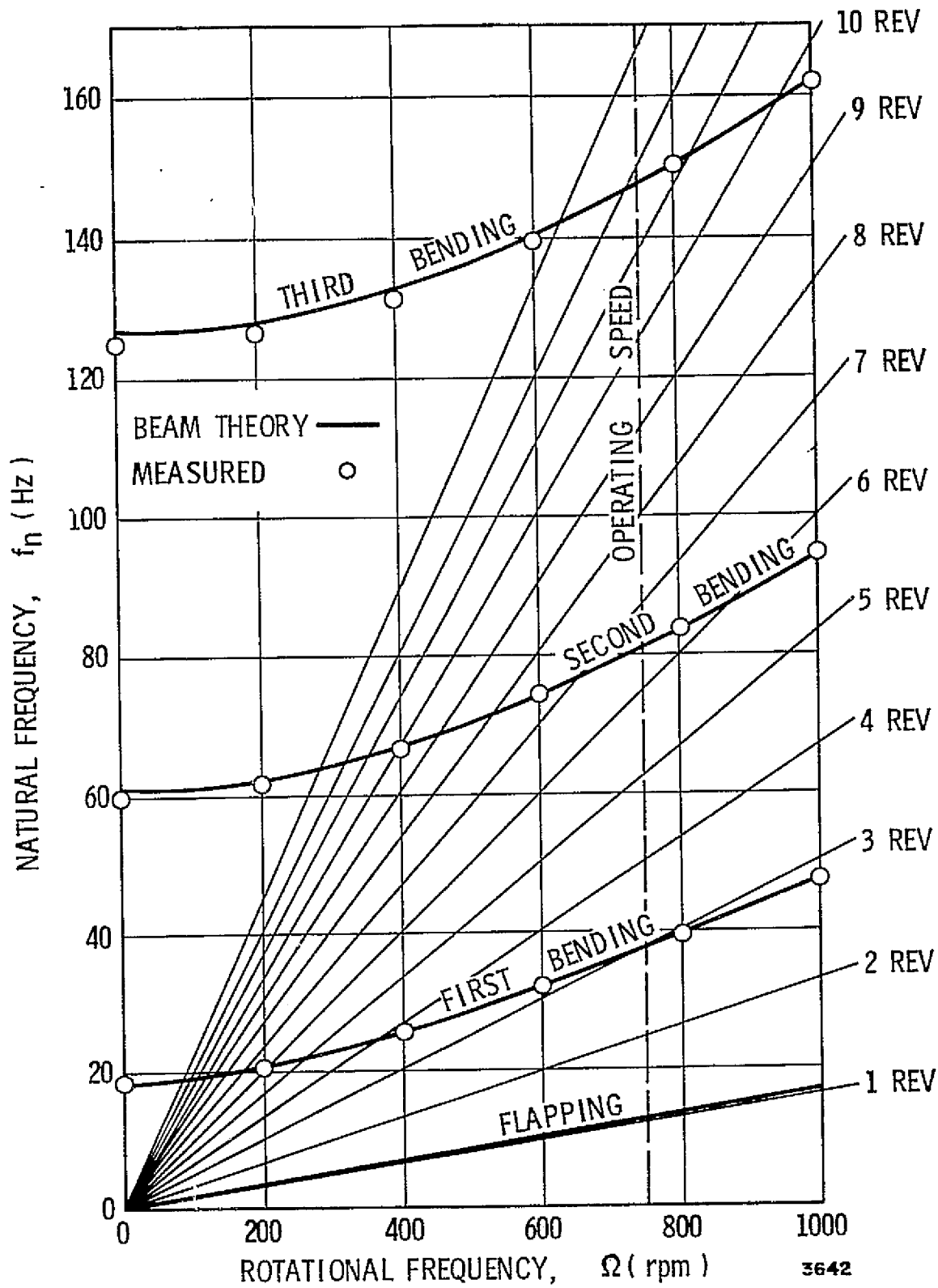
Figure 3. Natural Frequency Diagram of Model Helicopter
Rotor Blade
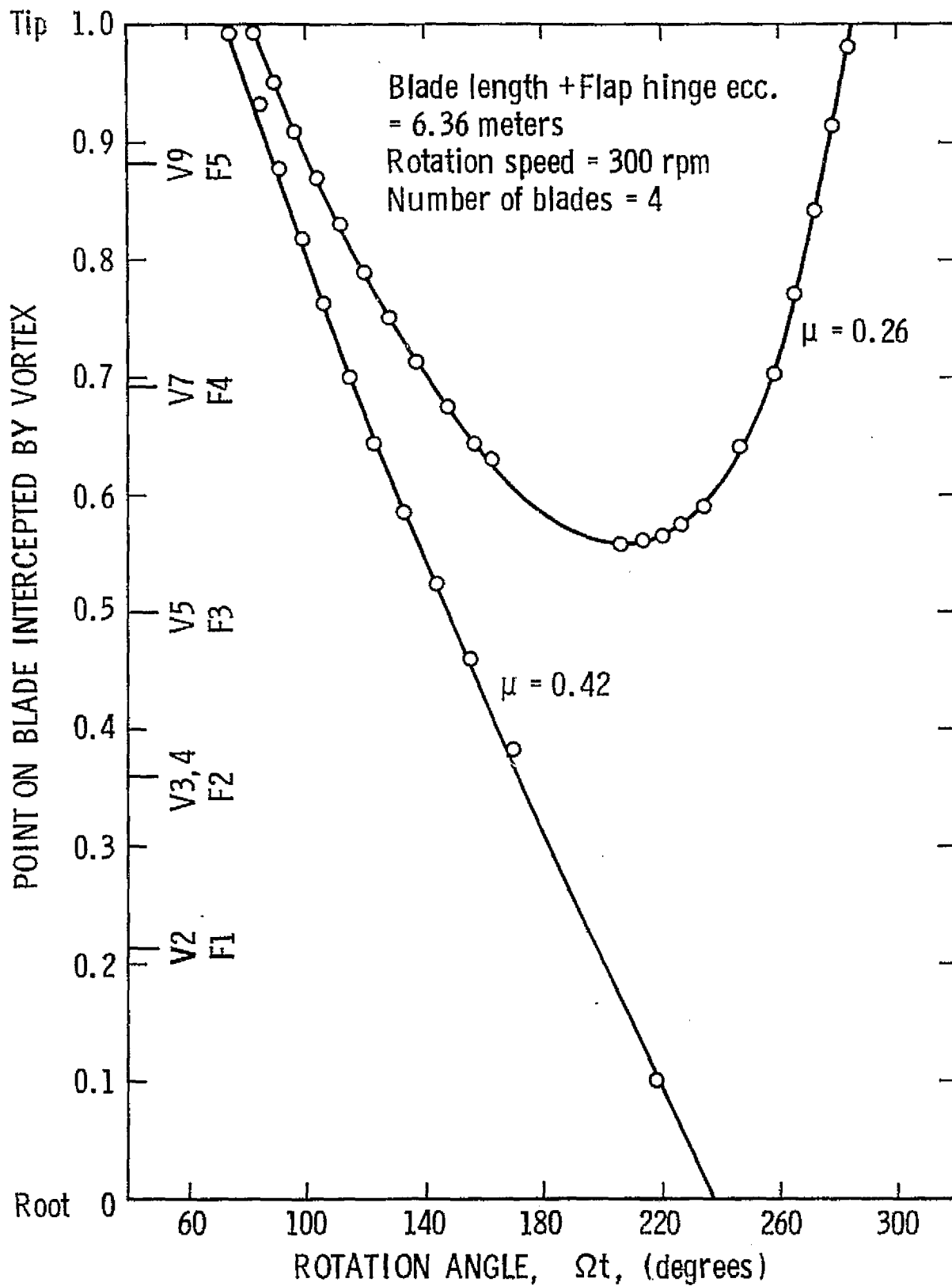
Figure 4. Intercept Point of Vortex on a Following Blade
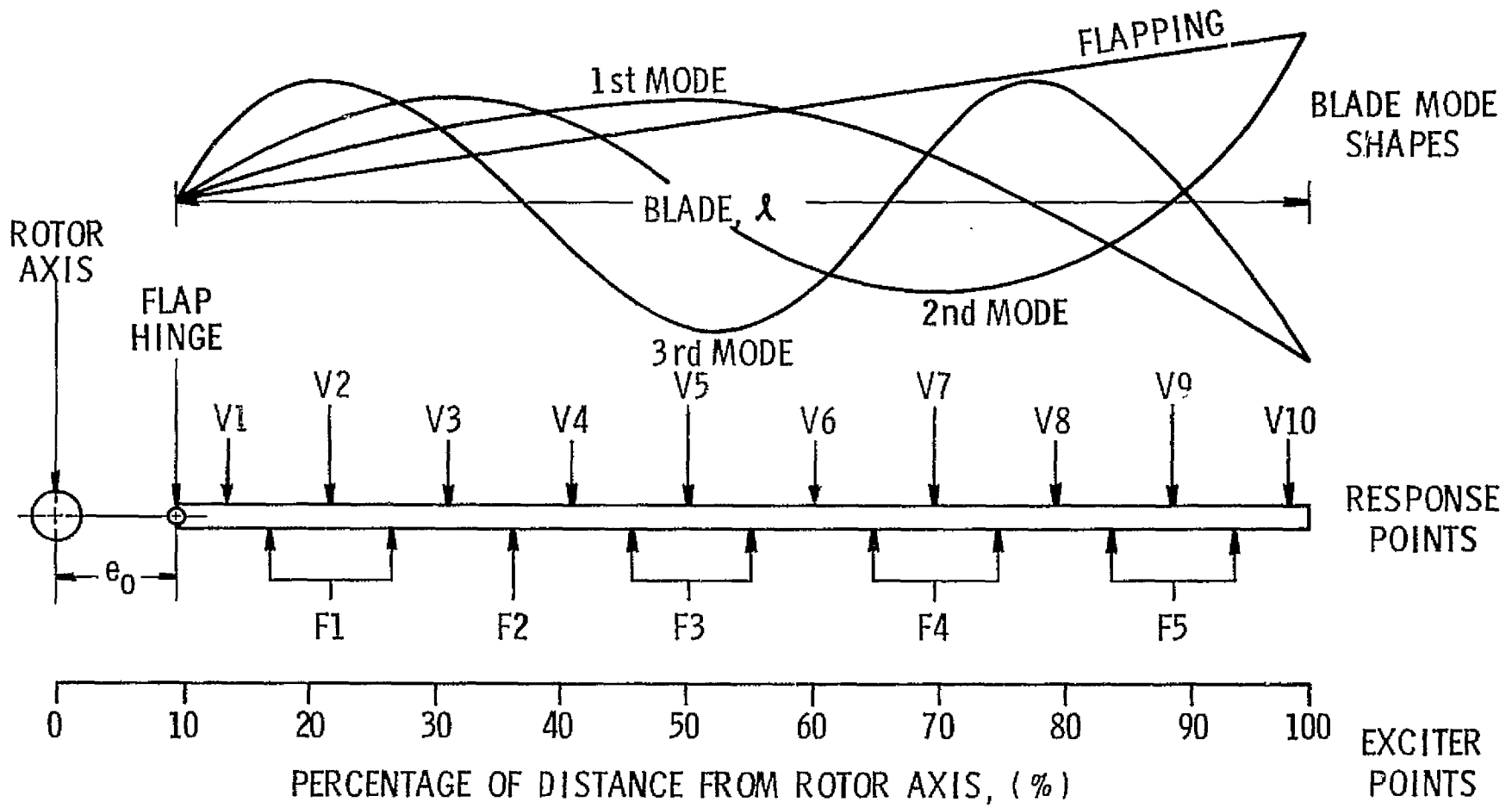
Figure 5.   Blade Mode Shapes and Location of Exciter and Response Points on Blade
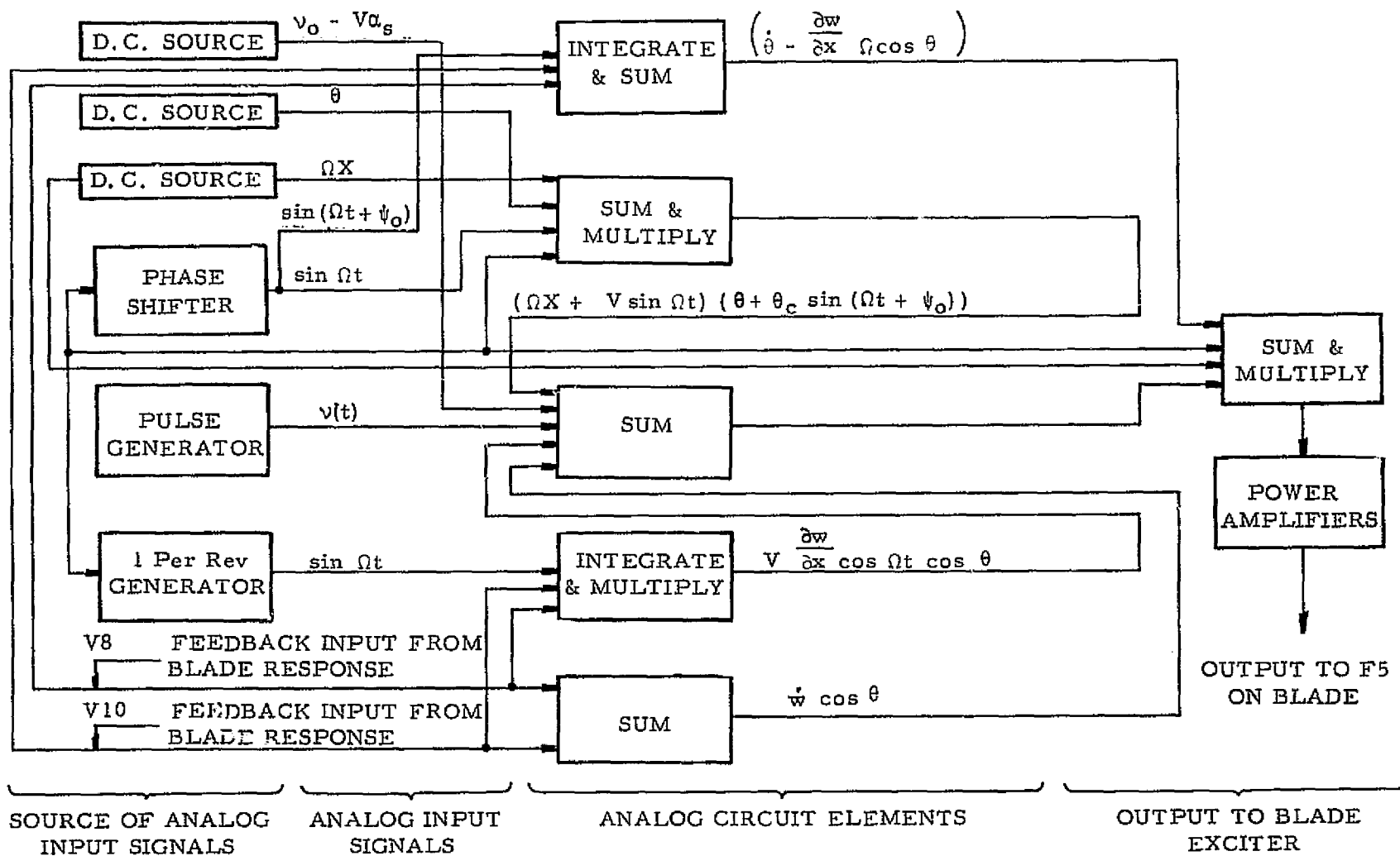
Figure 6. Block Diagram of Apparatus to Generate Excitation at F5

Timing Pulse at $\Omega t = 90°$
(1 per Rev)

(a) $\mu = 0.0$

0.18 m/sec, V7

0.18 m/sec, V9

1.02 x 10^3 Newtons, I_t

Timing Pulse
(1 per Rev)

(b) $\mu = 0.26$

1.81 m/sec, V7

0.90 m/sec, V9

2.56 x 10^3 Newtons, I_t

Timing Pulse
(1 per Rev)

(c) $\mu = 0.42$

1.81 m/sec, V7

1.81 m/sec, V9

5.12 x 10^3 Newtons, I_t
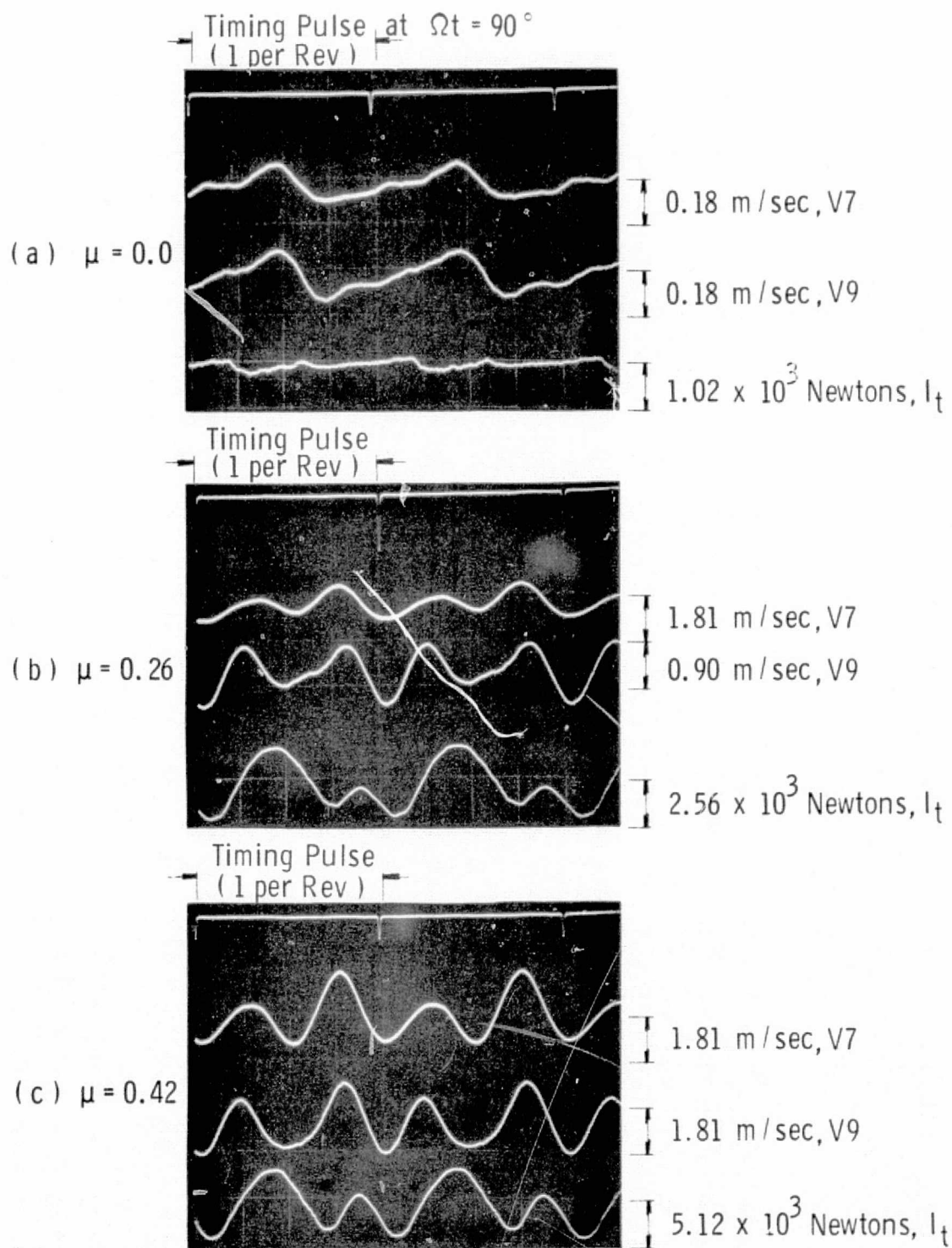
NOTE: V7 and V9 have different scale in Figure 7a
and Figures 7b and 7c

Figure 7. Response of Blade for Initial Conditions of Hover and
Forward Flight for Ω = 300 rpm ν(t) = 0 θ_0 = 12°,
No External Damping
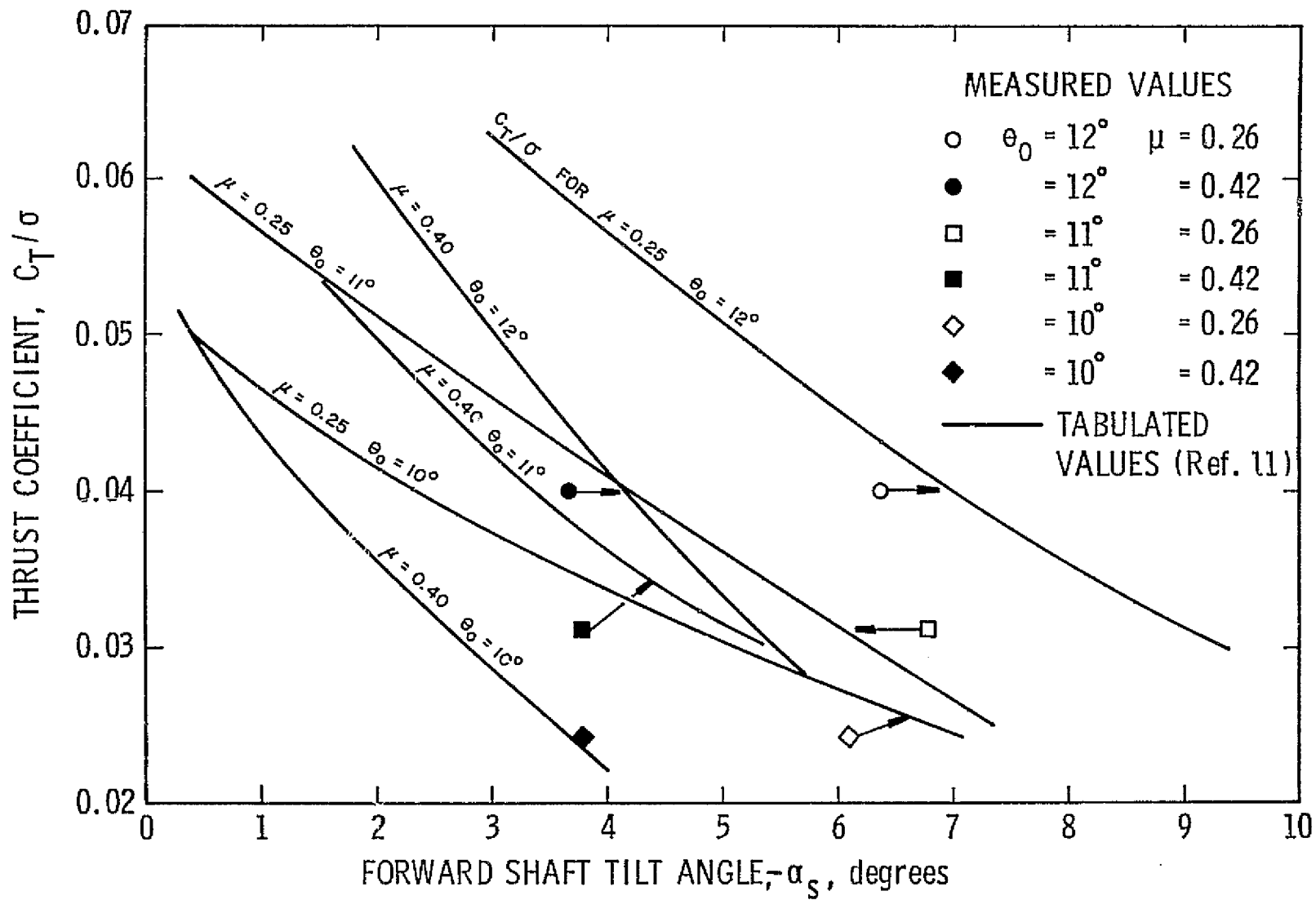
Figure 8. Comparison of Predicted and Modeled Thrust Coefficient
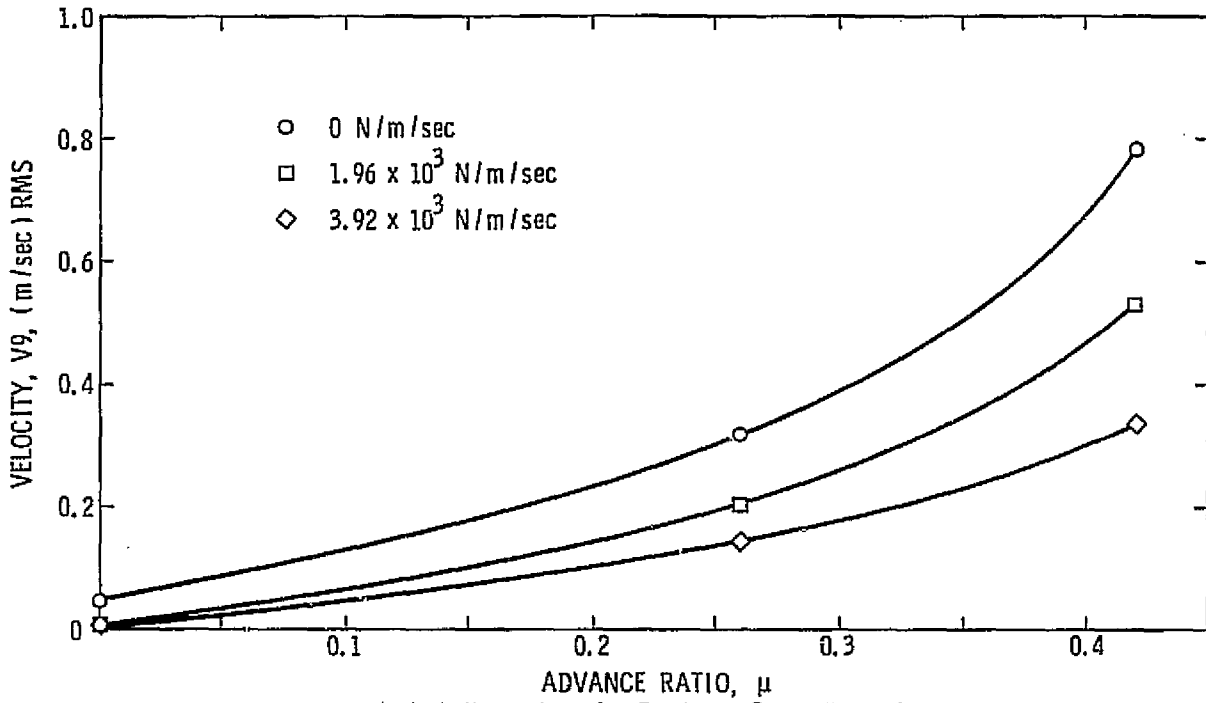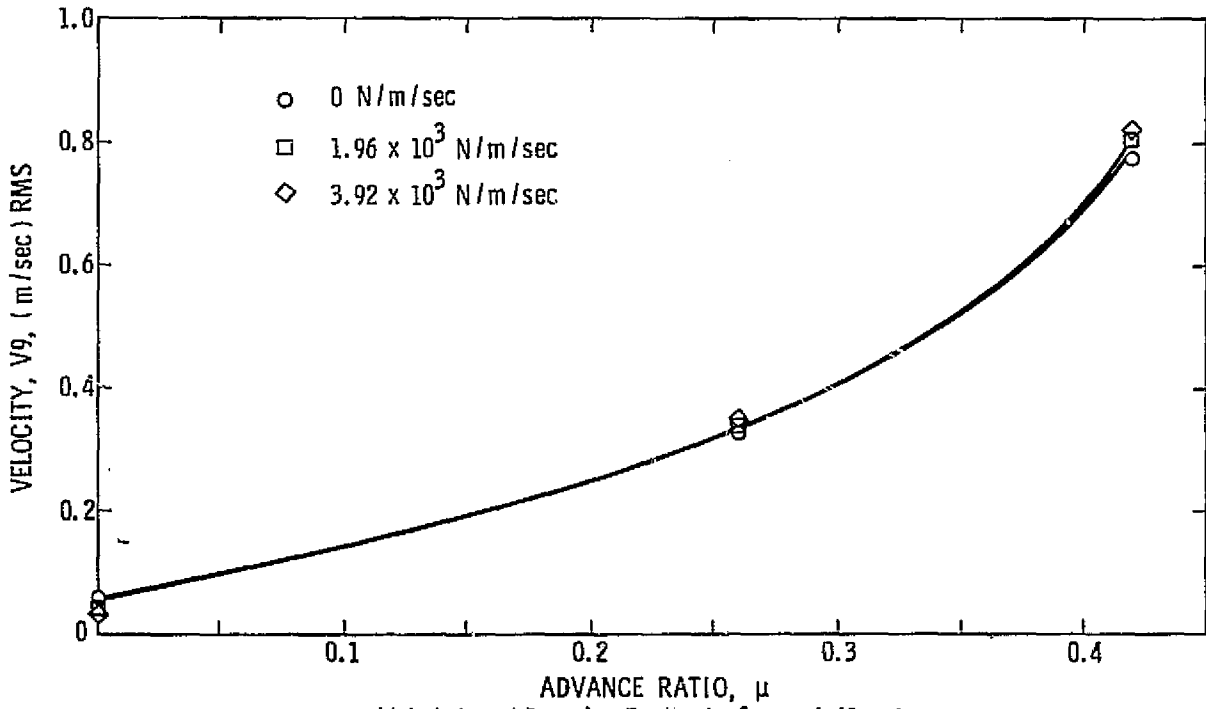
Figure 9. Blade V9 Response for $\theta_0 = 12°$, $\nu(t) = 0$, $p = 0$
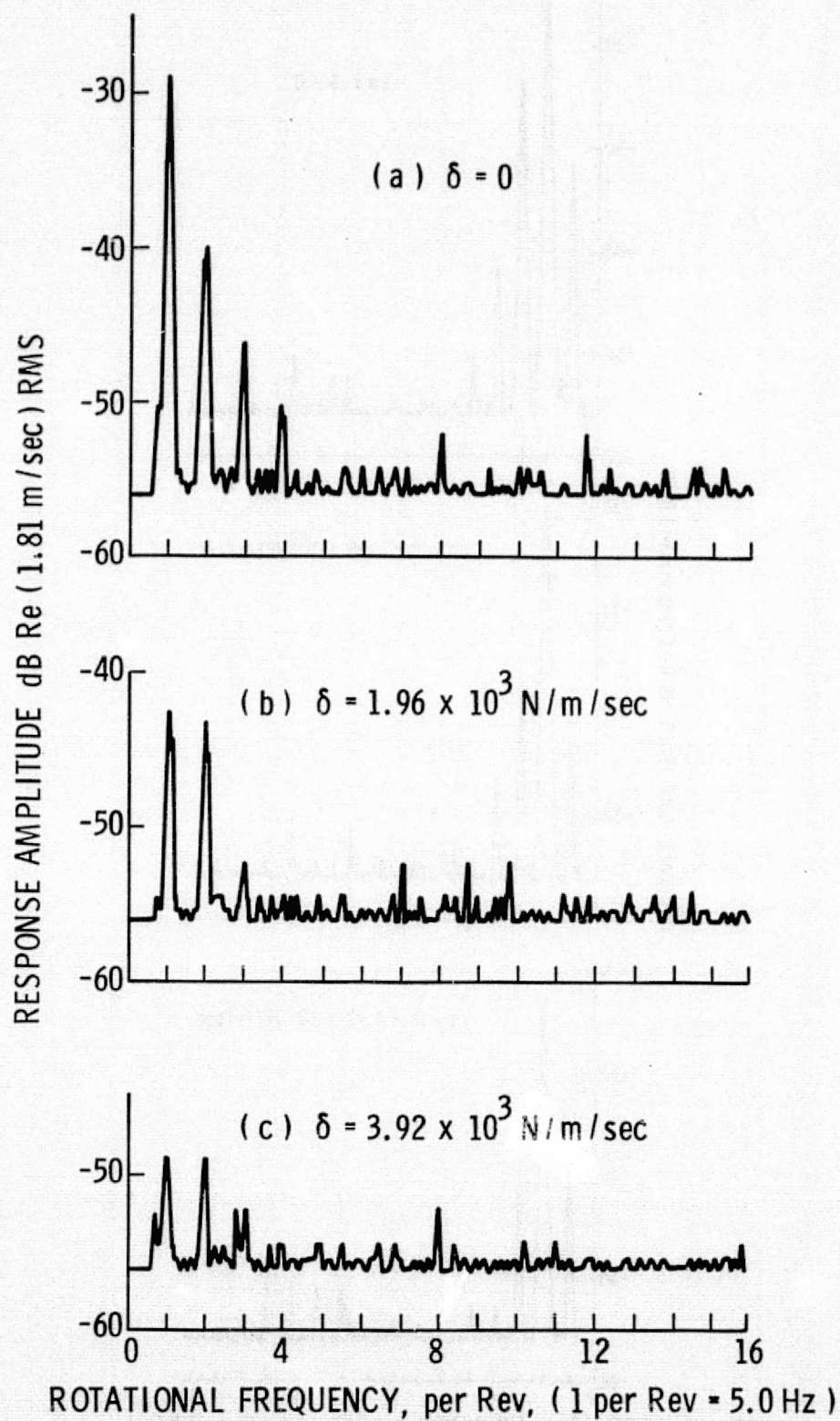
Figure 10. Spectral Plots of V9 Response, $\mu = 0$, $\nu(t) = 0$, $\theta_0 = 12°$, $p = 0$

41
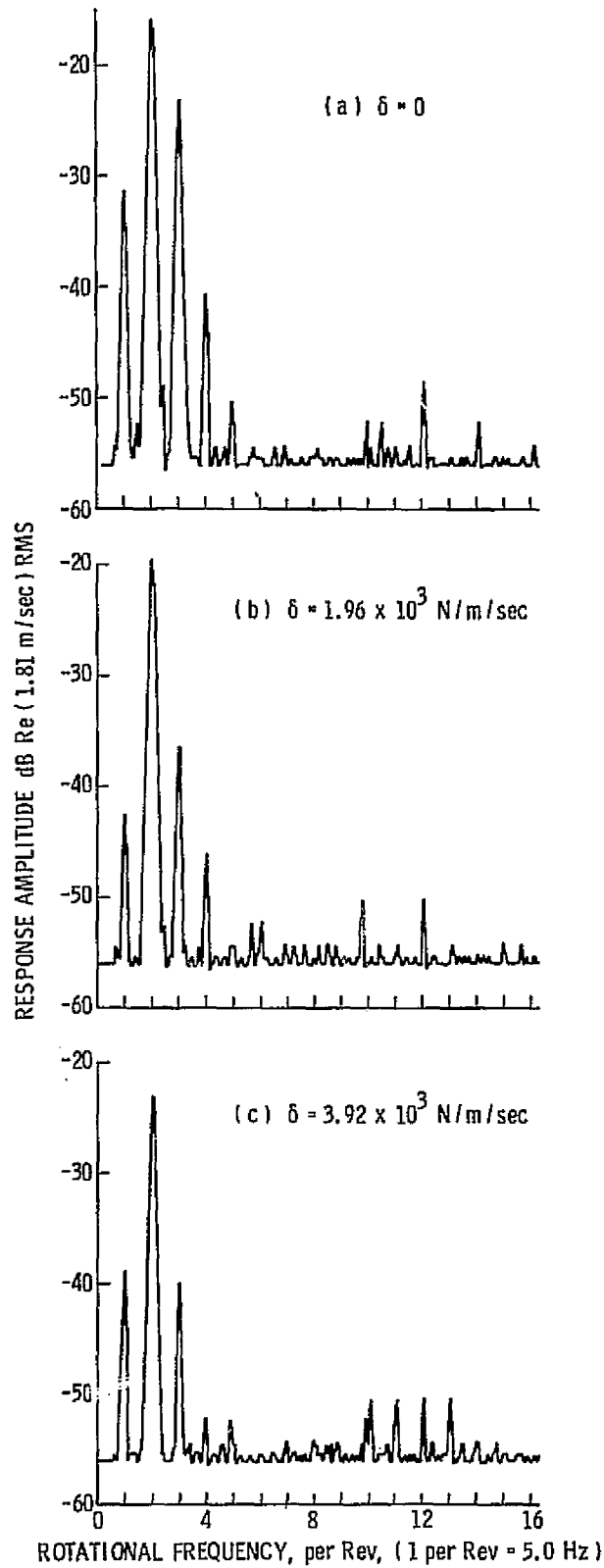
Figure 11. Spectral Plots of V9 Response, $\mu = 0.26$, $\nu(t) = 0$, $\theta_0 = 12°$, $p = 0$
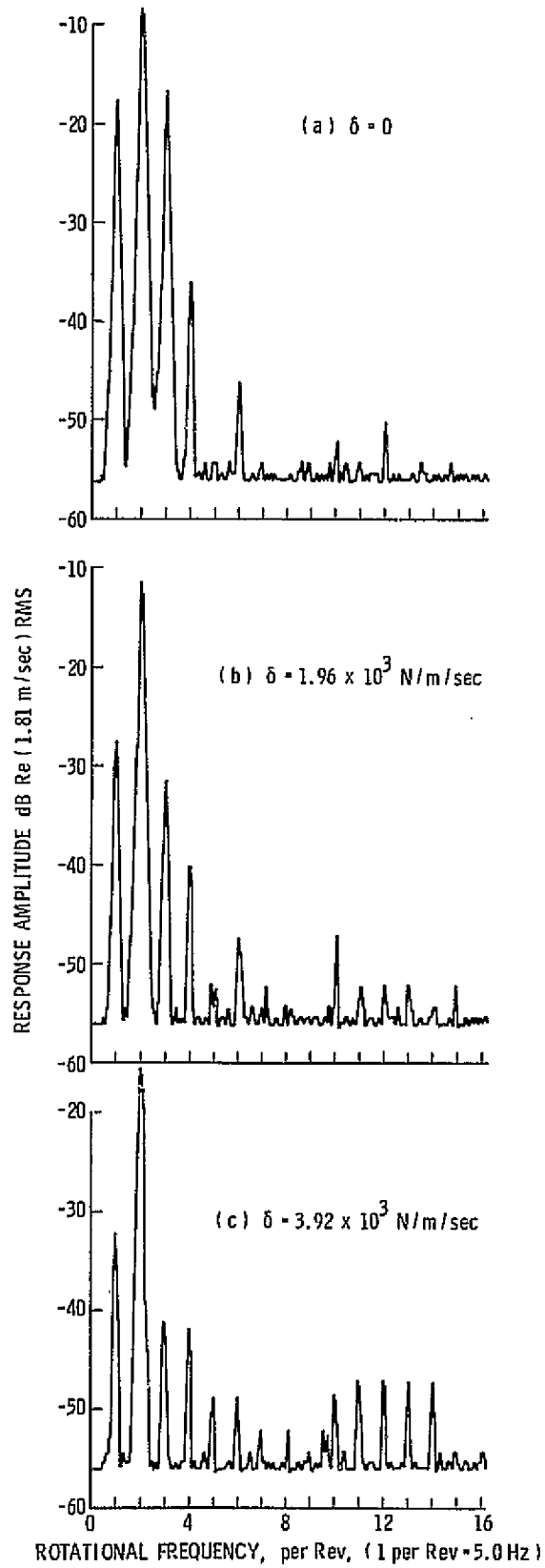
Figure 12. Spectral Plots of V9 Response, $\mu = 0.42$, $\nu(t) = 0$, $\theta_0 = 12°$, $p = 0$

Timing Pulse at $\Omega t \approx 90°$
(1 per Rev)

(a) $\mu = 0.0$

1.81 m/sec, V7

1.81 m/sec, V9

5.12 x 10^3 Newtons, I_t
p = 1, Pulse Applied

Timing Pulse
(1 per Rev)

(b) $\mu = 0.42$

1.81 m/sec, V7

1.81 m/sec, V9

5.12 x 10^3 Newtons, I_t
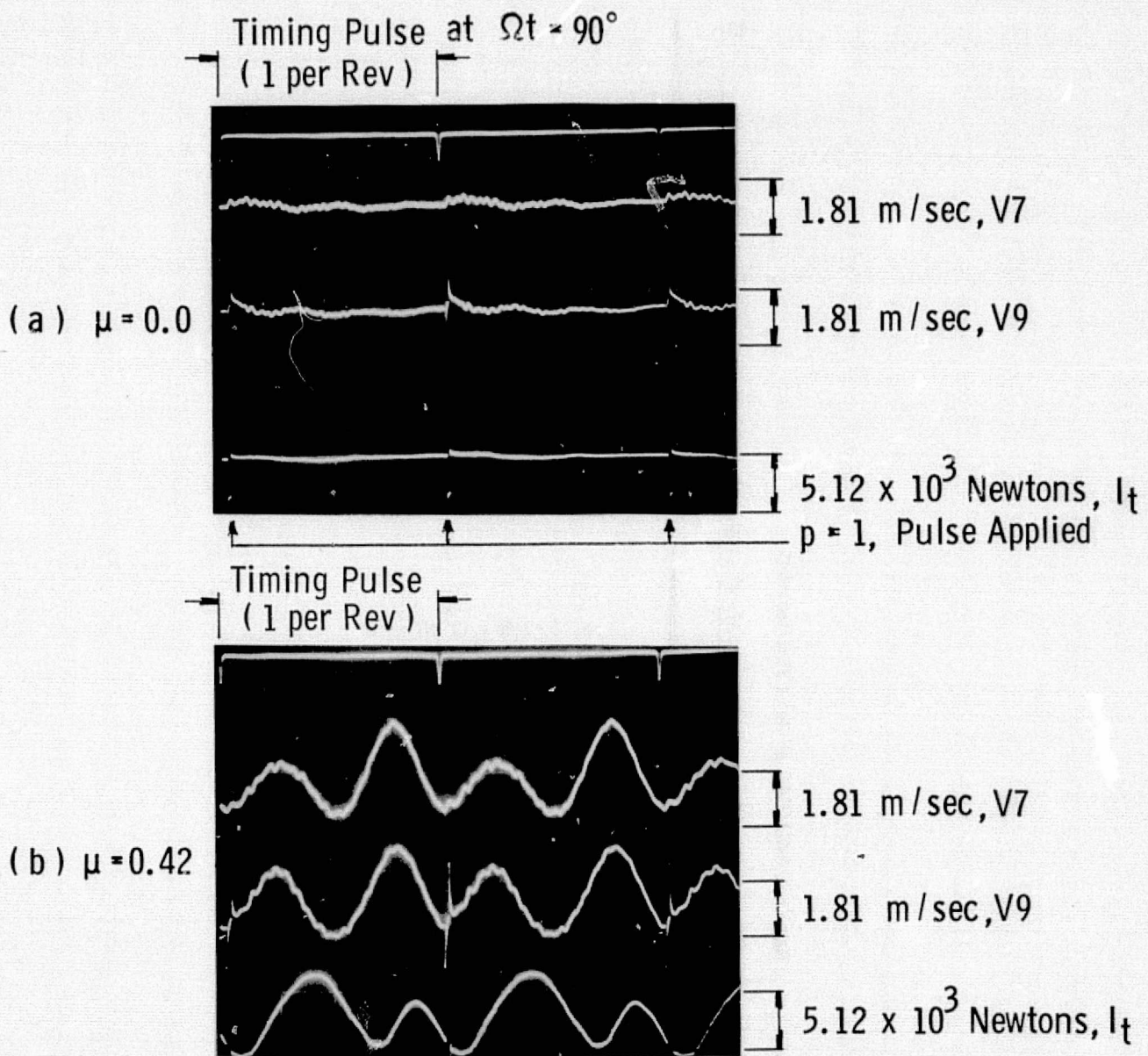
Figure 13. Response of Blade V7, V9 for $\Omega = 300$ rpm
$\nu(t) = 1$ per Rev Pulse, $\theta_0 = 12°$, No External Damping
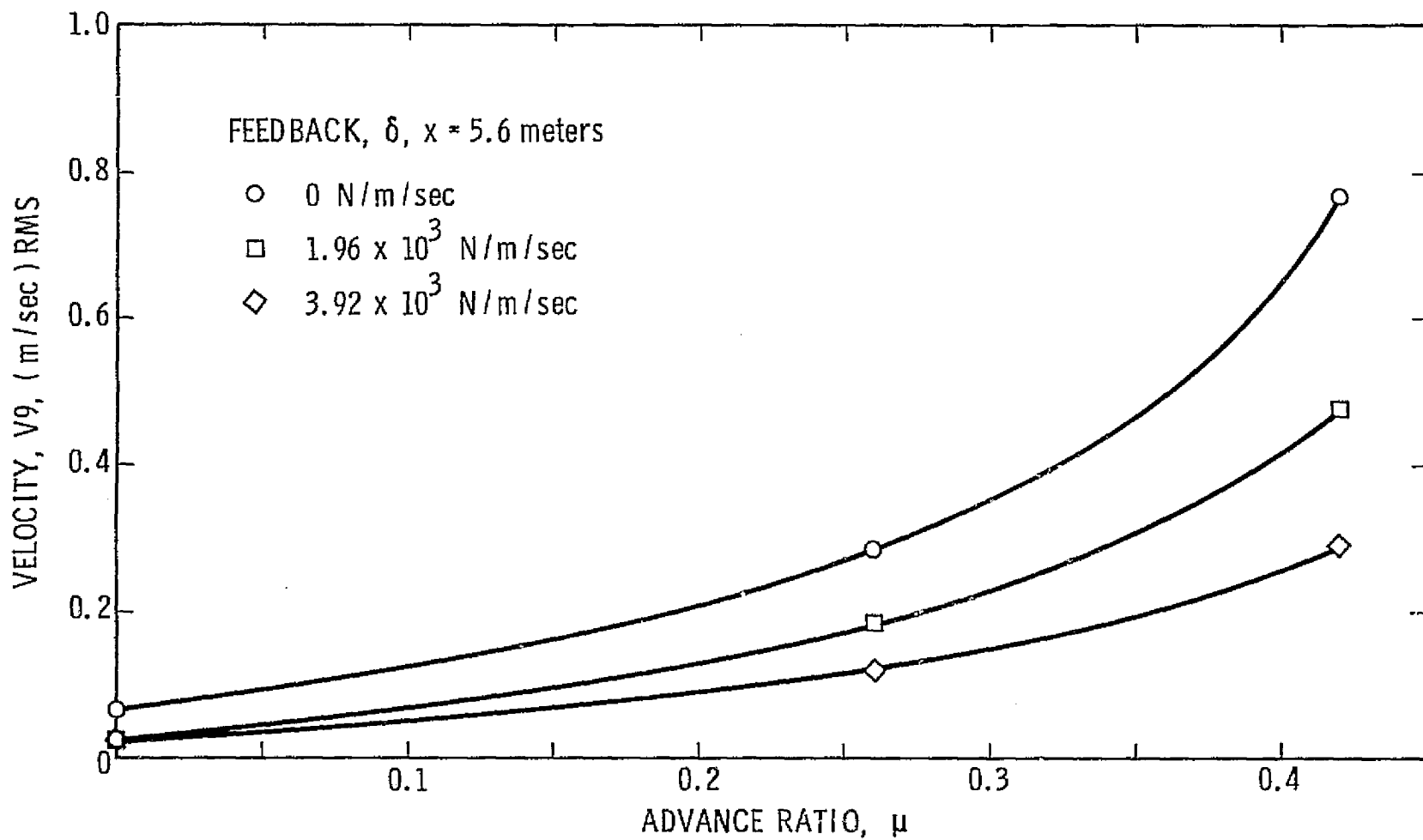
Figure 14. Blade V9 Response for Outboard Damping $\theta_0 = 12°$, $\nu(t) = 1$ per Rev Pulse ($p = 1$)
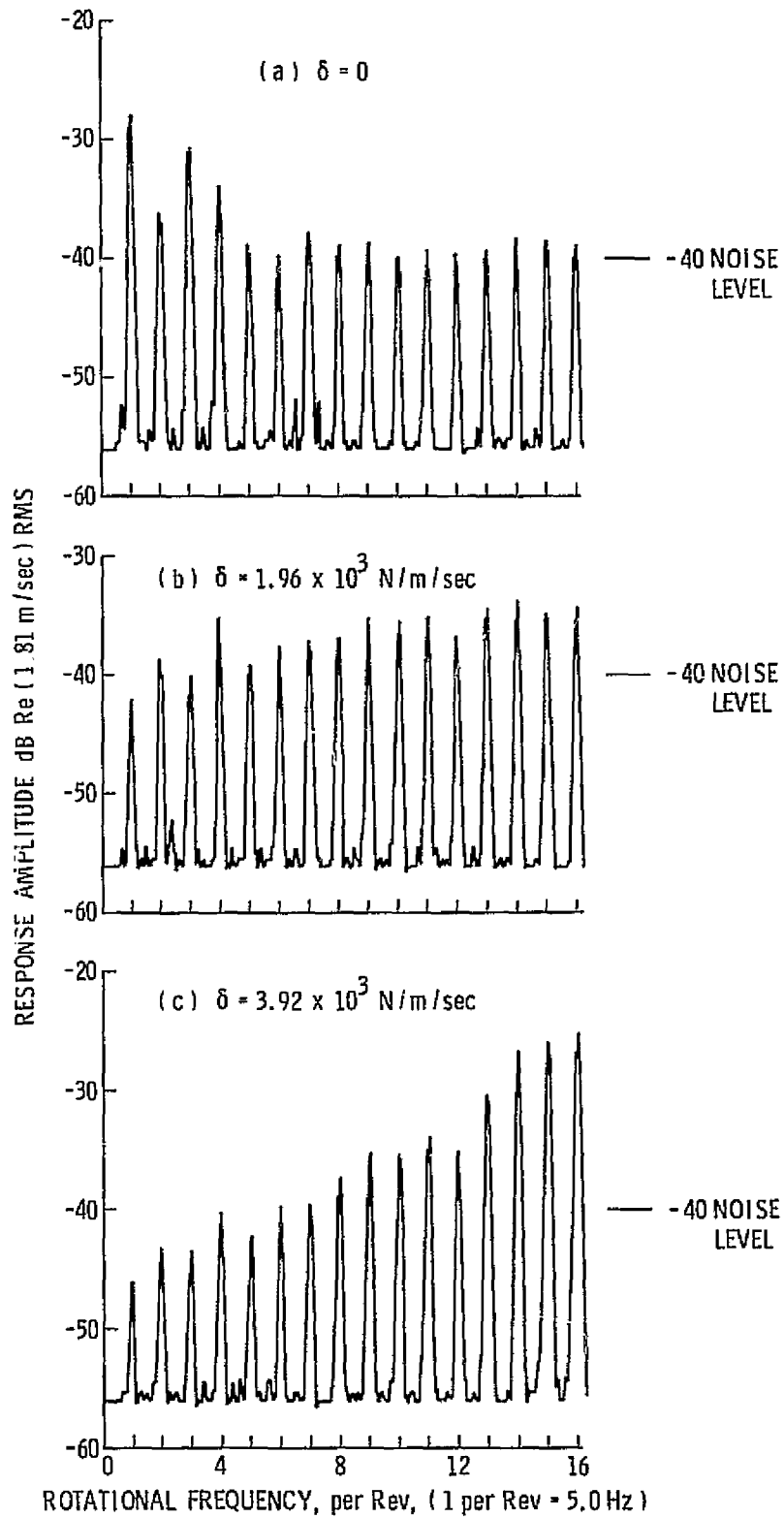
Figure 15. Spectral Plot of V9 Response, $\mu = 0$, $\nu(t) = 1$ per Rev, $\theta_0 = 12°$, $p = 1$
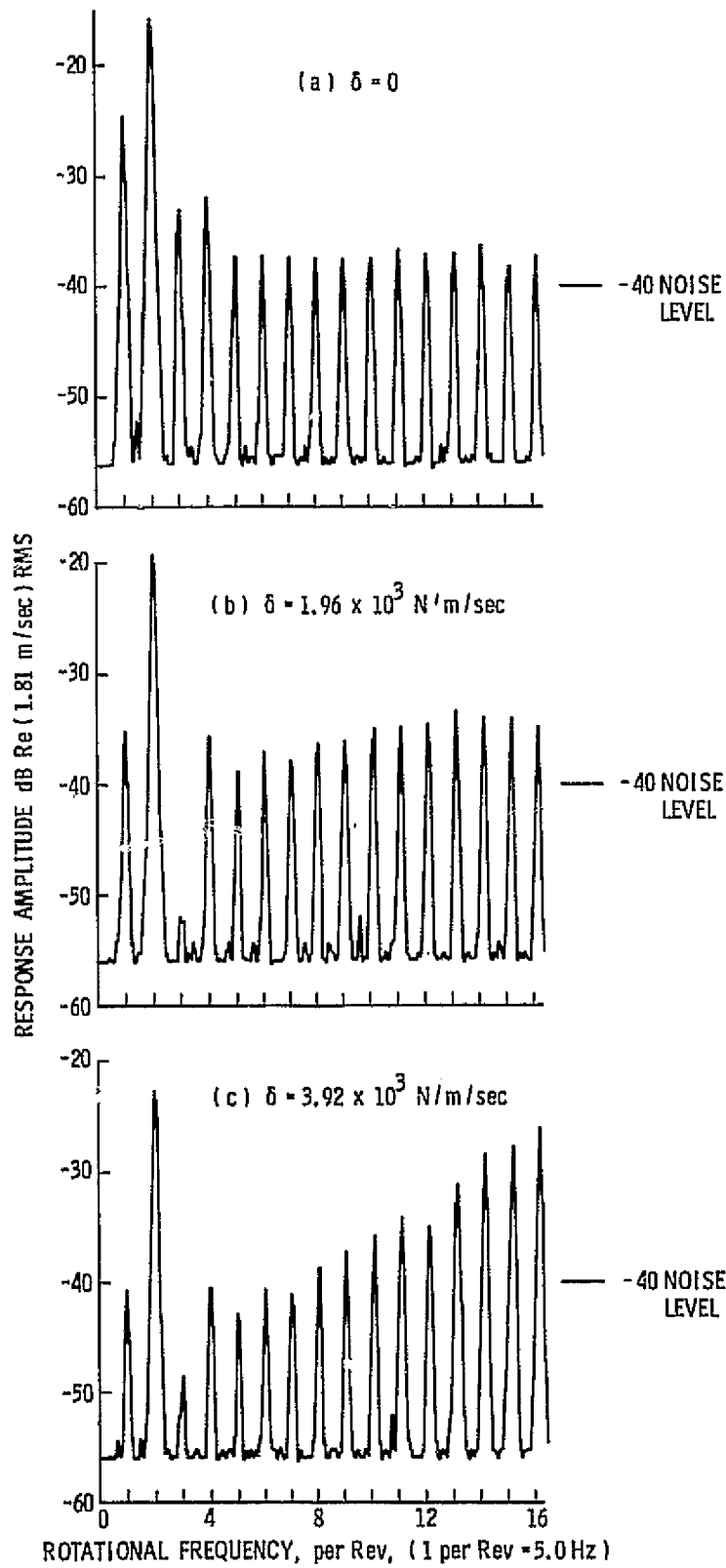
Figure 16. Spectral Plot of V9 Response, $\mu = 0.26$, $\nu(t) = 1$ per Rev, $\theta_0 = 12°$, $p = 1$
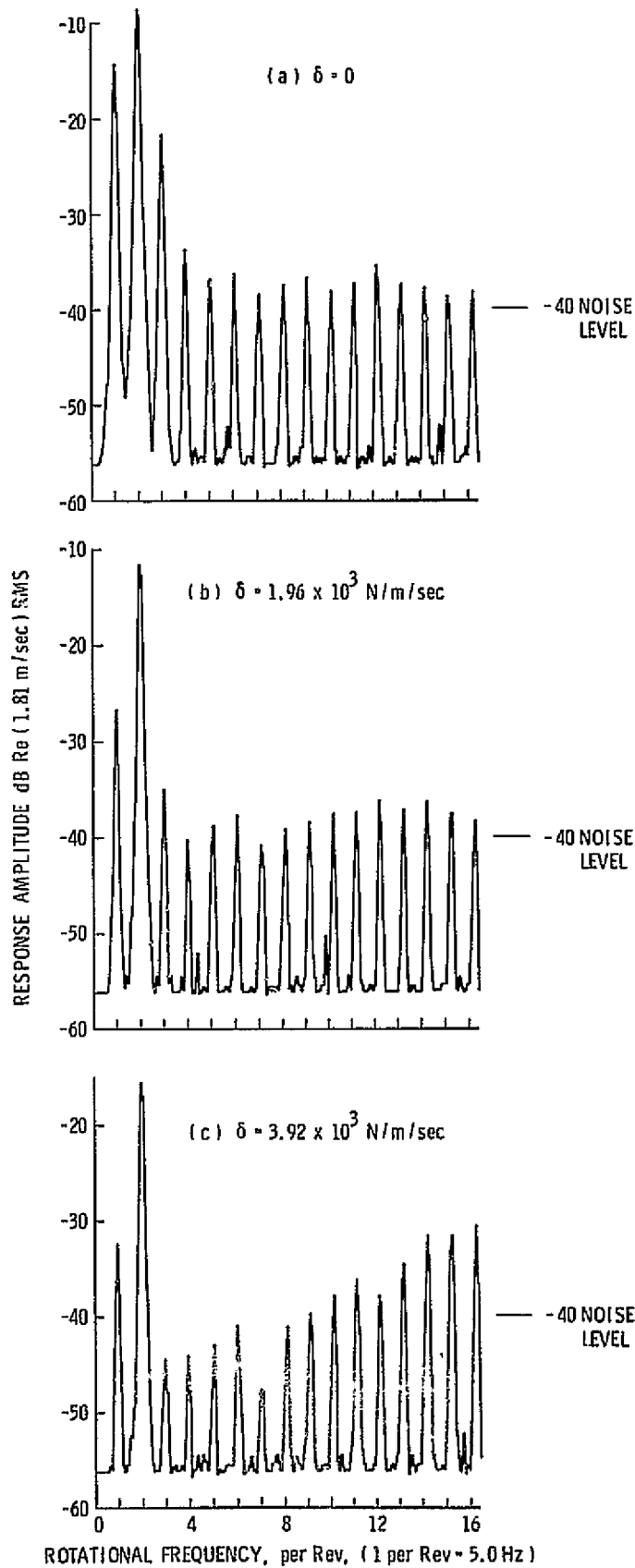
Figure 17. Spectral Plot of V9 Response, $\mu = 0.42$, $\nu(t) = 1$ per Rev, $\theta_0 = 12°$, $p = 1$

48
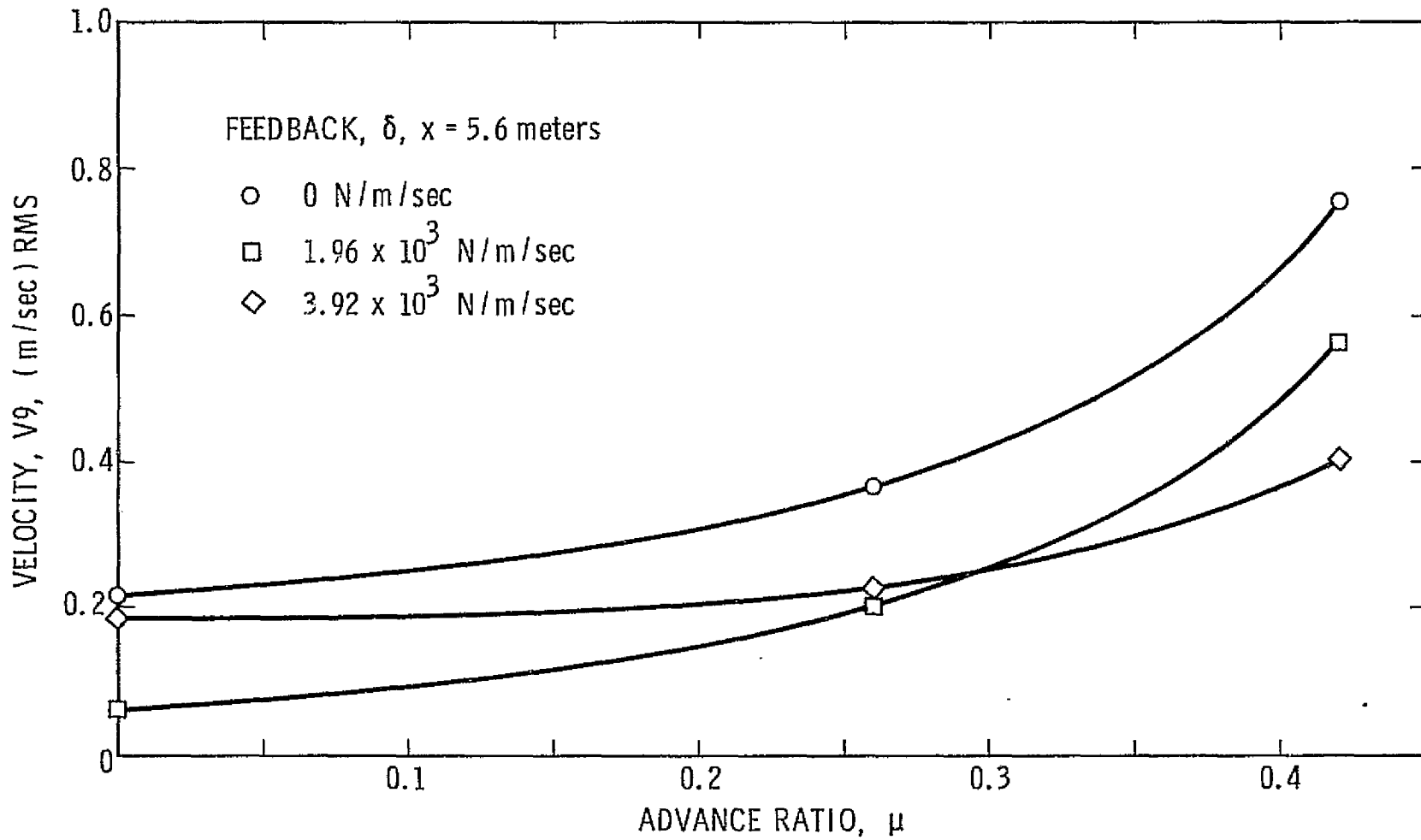
Figure 18. Blade V9 Resposne for Outboard Damping $\theta_0 = 12°$, $\nu(t) = 1$ per Rev Pulse ($p = 3$)
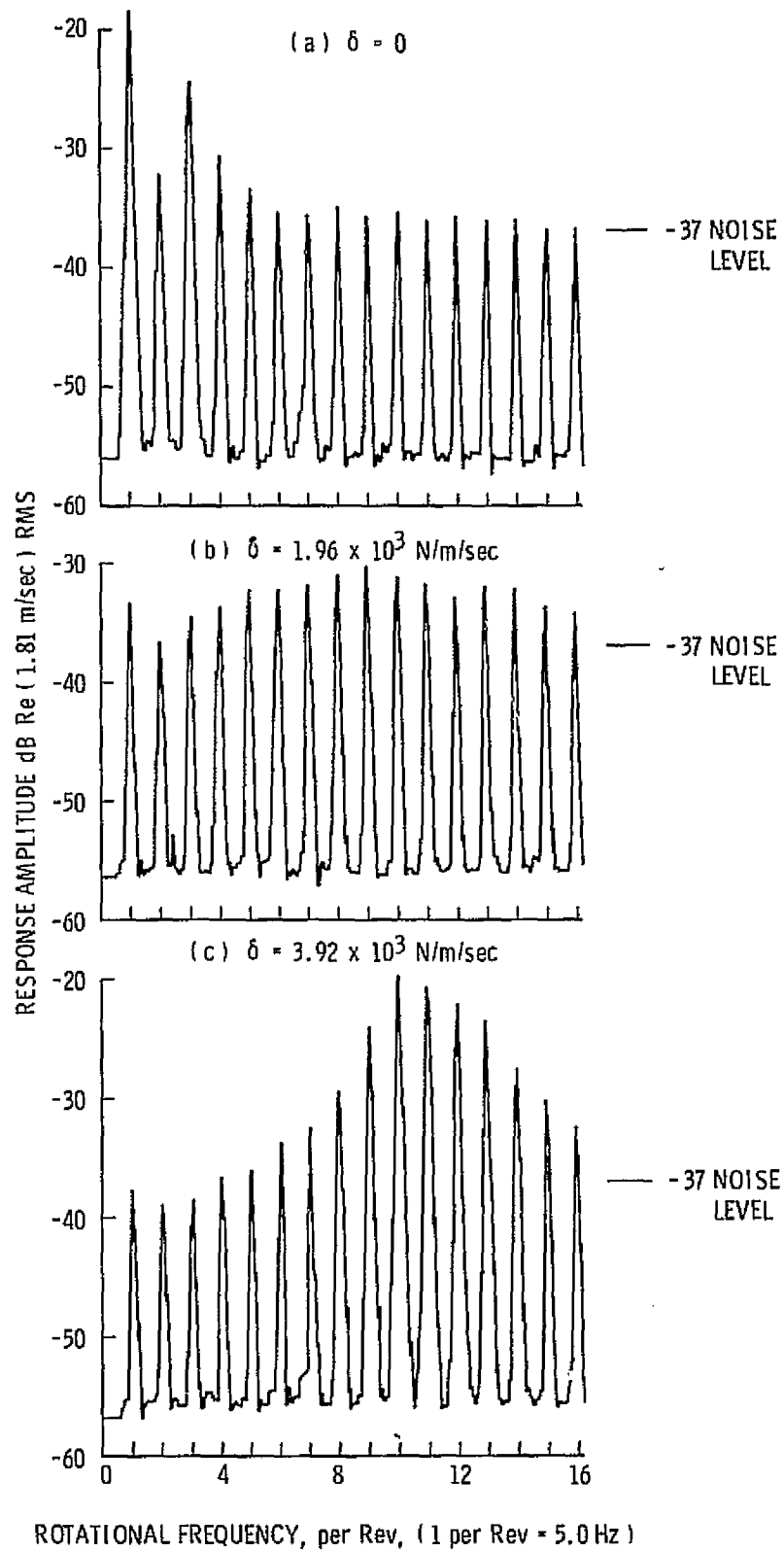
Figure 19. Spectral Plots of V9 Response, $\mu = 0.0$, $\nu(t) = 1$ per Rev, $\theta_0 = 12°$, $p = 3$
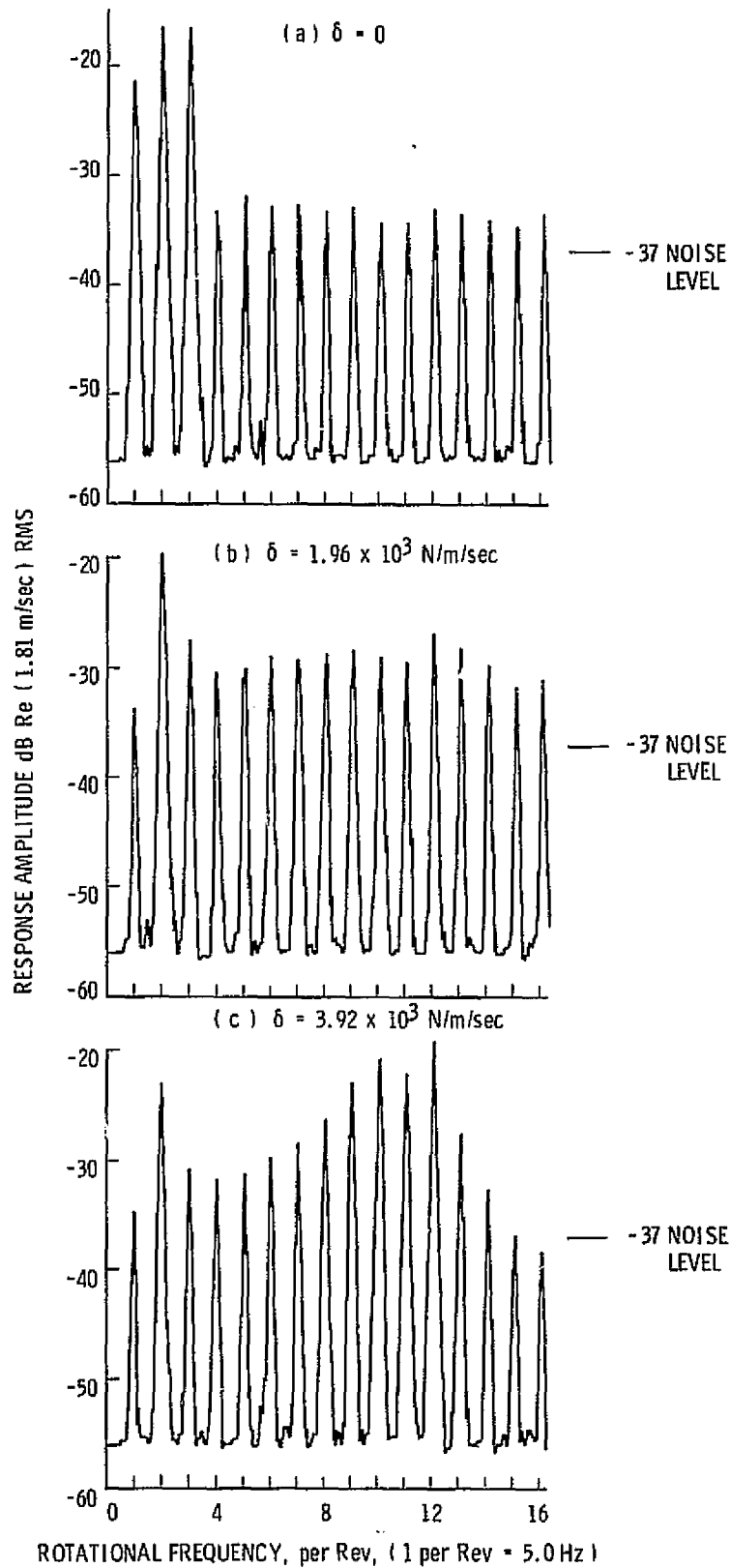
Figure 20. Spectral Plots of V9 Response, $\mu = 0.26$, $\nu(t) = 1$ per Rev, $\theta_0 = 12°$, $p = 3$
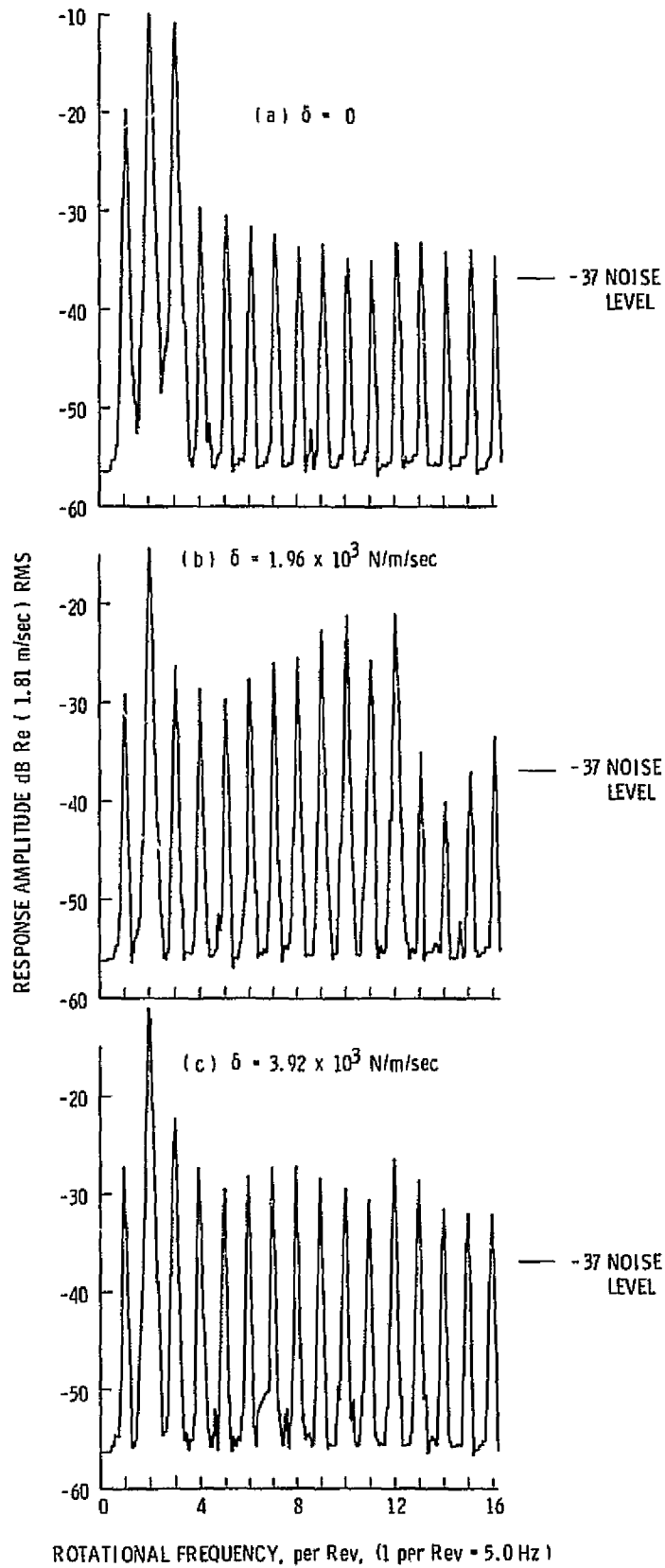
Figure 21. Spectral Plots of V9 Response, $\mu = 0.42$, $\nu(t) = 1$ per Rev, $\theta_0 = 12°$, $p = 3$
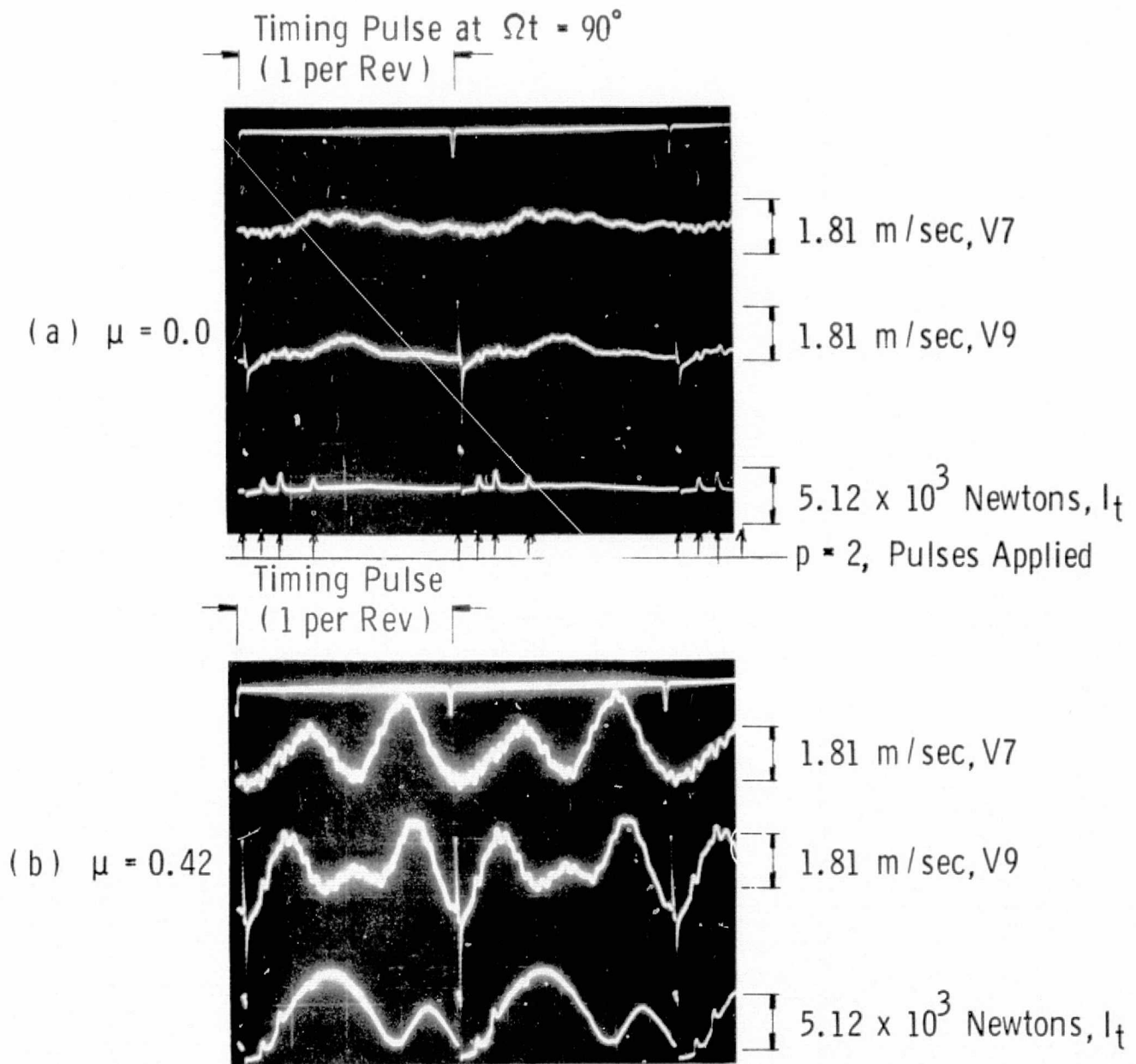
Figure 22. Response of Blade: V7, V9 versus Time for $\Omega = 300$ rpm
$\nu(t) =$ Moving Pulse, $\theta_0 = 12°$, No External Damping
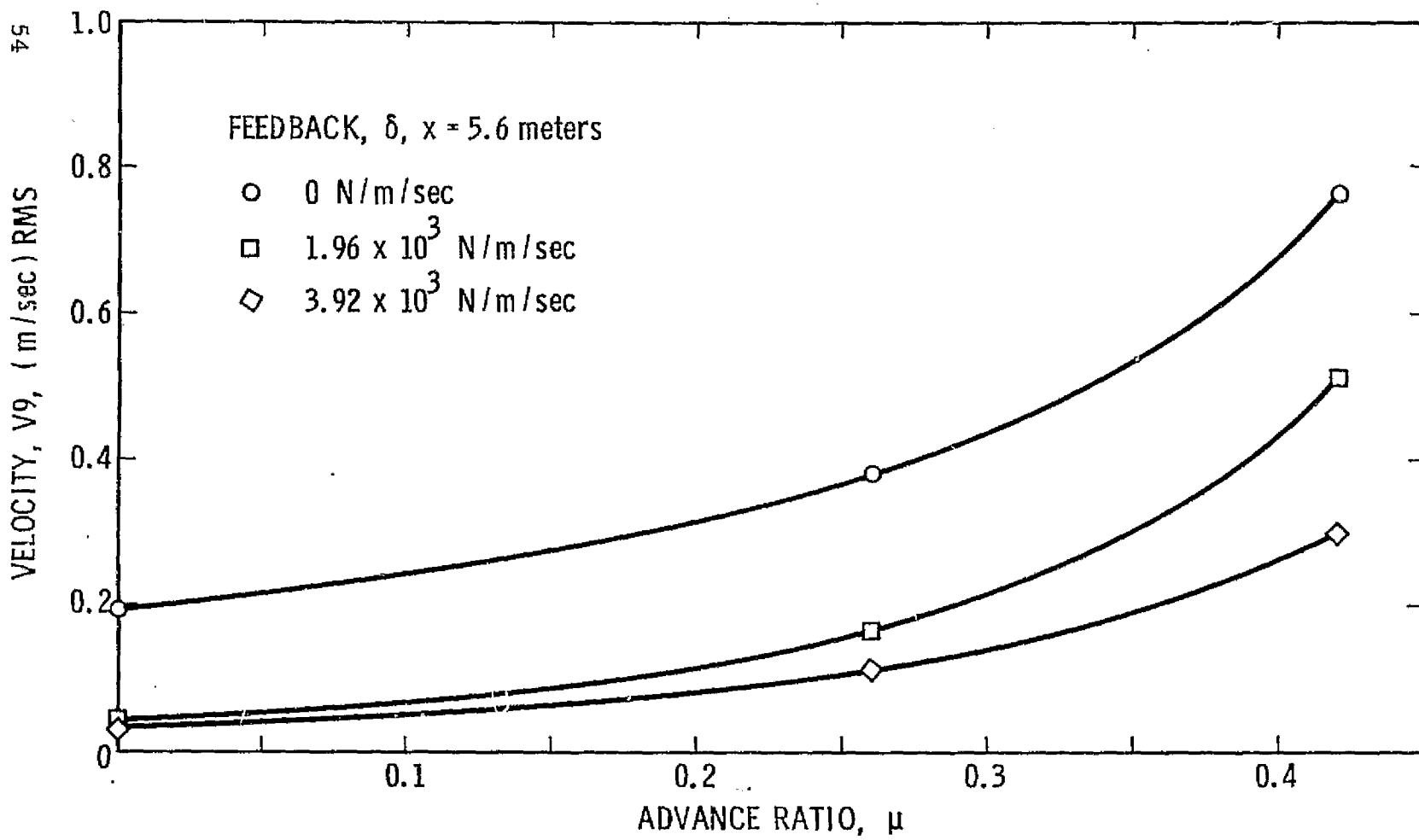
Figure 23. Blade V9 Response for Outboard Damping $\theta_0 = 12°$, $v(t)$ = Moving Pulse (p = 2)
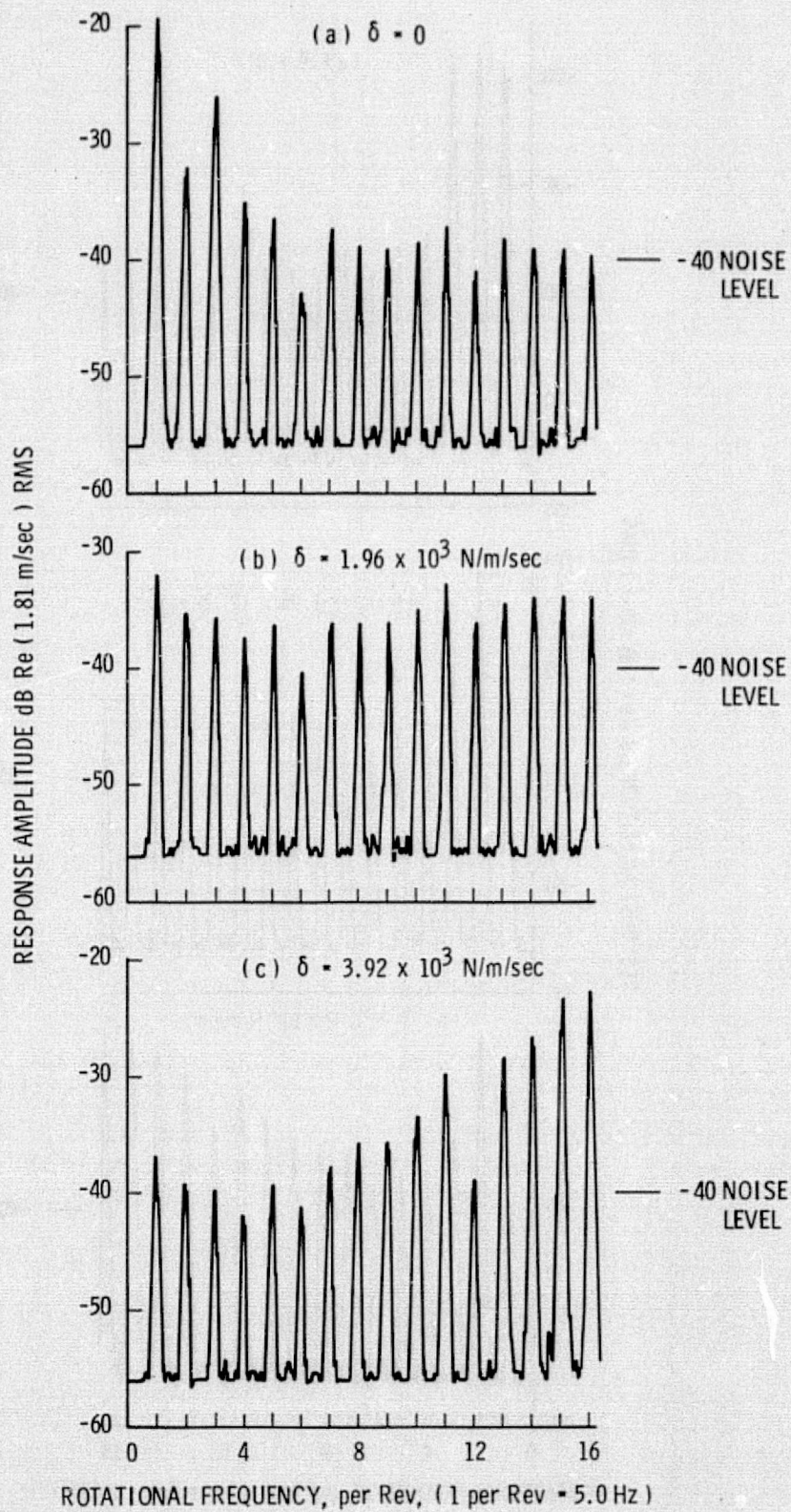
Figure 24. Spectral Plots of V9 Response, $\mu = 0$, $\nu(t) = $ moving pulse, $\theta_0 = 12°$, $p = 2$
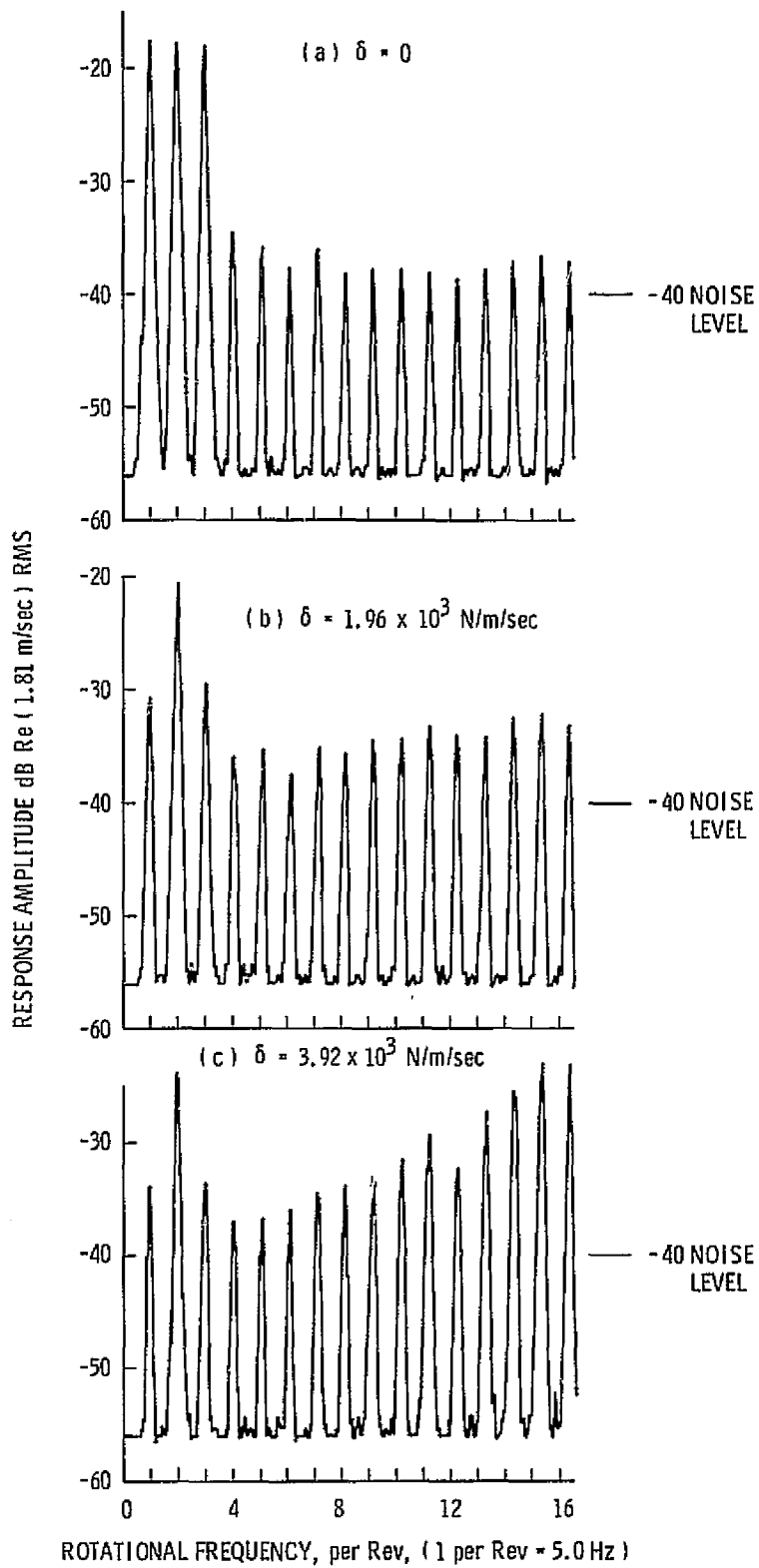
Figure 25. Spectral Plots of V9 Response, $\mu = 0.26$, $\nu(t)$ = moving pulse, $\theta_0 = 12°$, $p = 2$
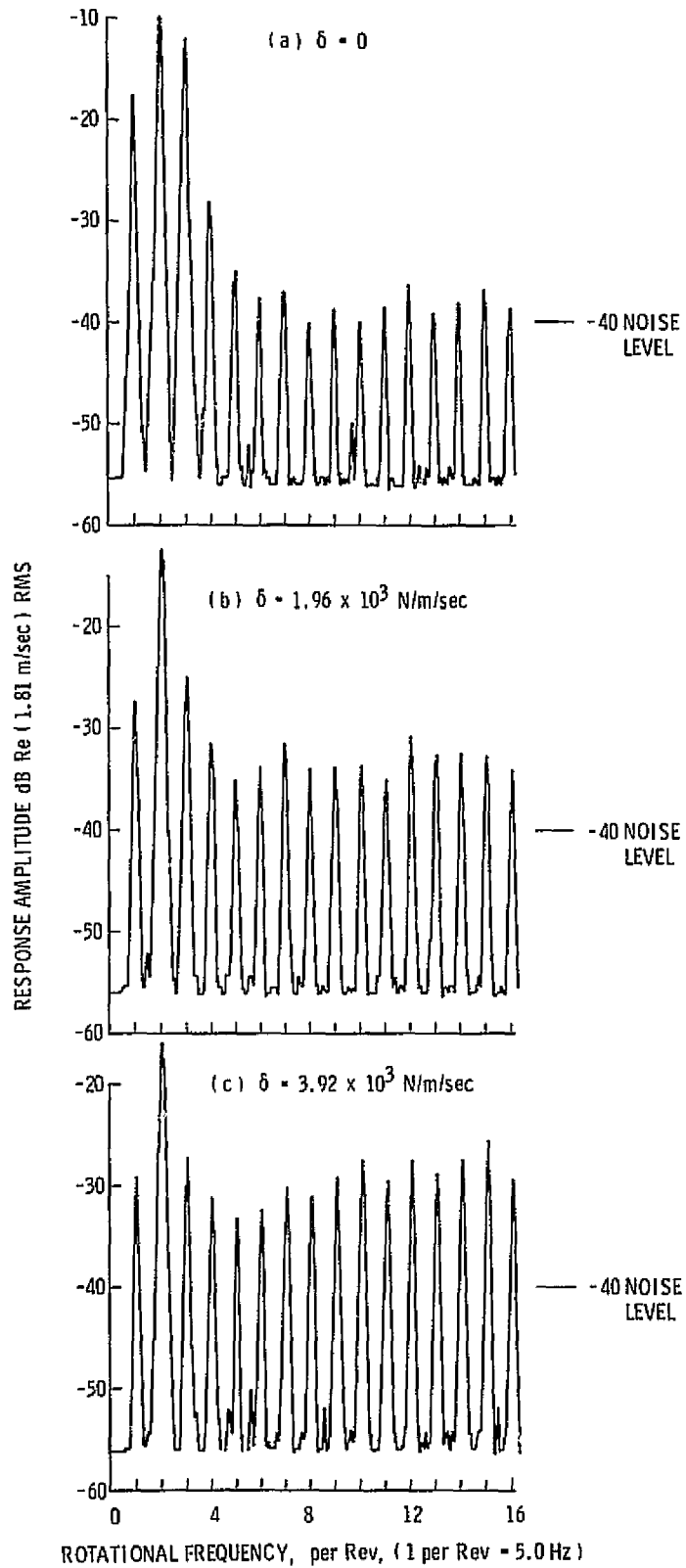
Figure 26. Spectral Plots of V9 Response, $\mu = 0.42$, $\nu(t)$ = moving pulse, $\theta_0 = 12°$, $p = 2$
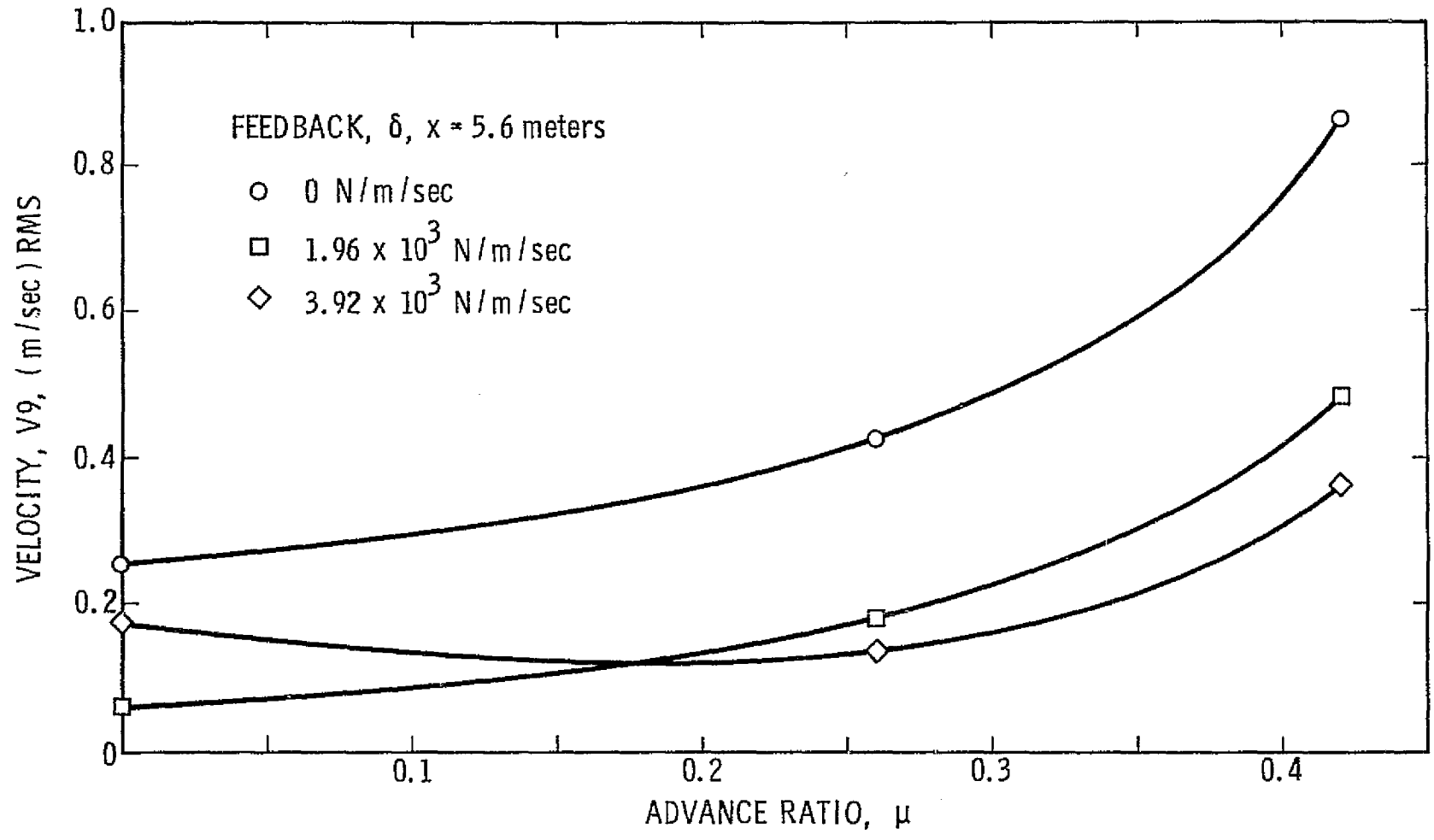
Figure 27. Blade V9 Response for Outboard Damping $\theta_0 = 12°$, $\nu(t)$ = Moving Pulse ($p = 4$)

The chart shows VELOCITY, V9, (m/sec) RMS on the vertical axis (0 to 1.0) versus ADVANCE RATIO, μ on the horizontal axis (0 to 0.4).

FEEDBACK, δ, x = 5.6 meters

- ○ 0 N/m/sec
- □ 1.96×10^3 N/m/sec
- ◇ 3.92×10^3 N/m/sec

Figure 28. Spectral Plots of V9 Response, $\mu = 0.0$, $\nu(t) = \theta_0 = 12°$, $p = 4$

(a) δ = 0

− 36 NOISE
LEVEL

(b) δ = 1.96 x 10³ N/m/sec

− 36 NOISE
LEVEL

(c) δ = 3.92 x 10³ N/m/sec

− 36 NOISE
LEVEL

RESPONSE AMPLITUDE dB Re (1.81 m/sec) RMS

ROTATIONAL FREQUENCY, per Rev, (1 per Rev = 5.0 Hz)
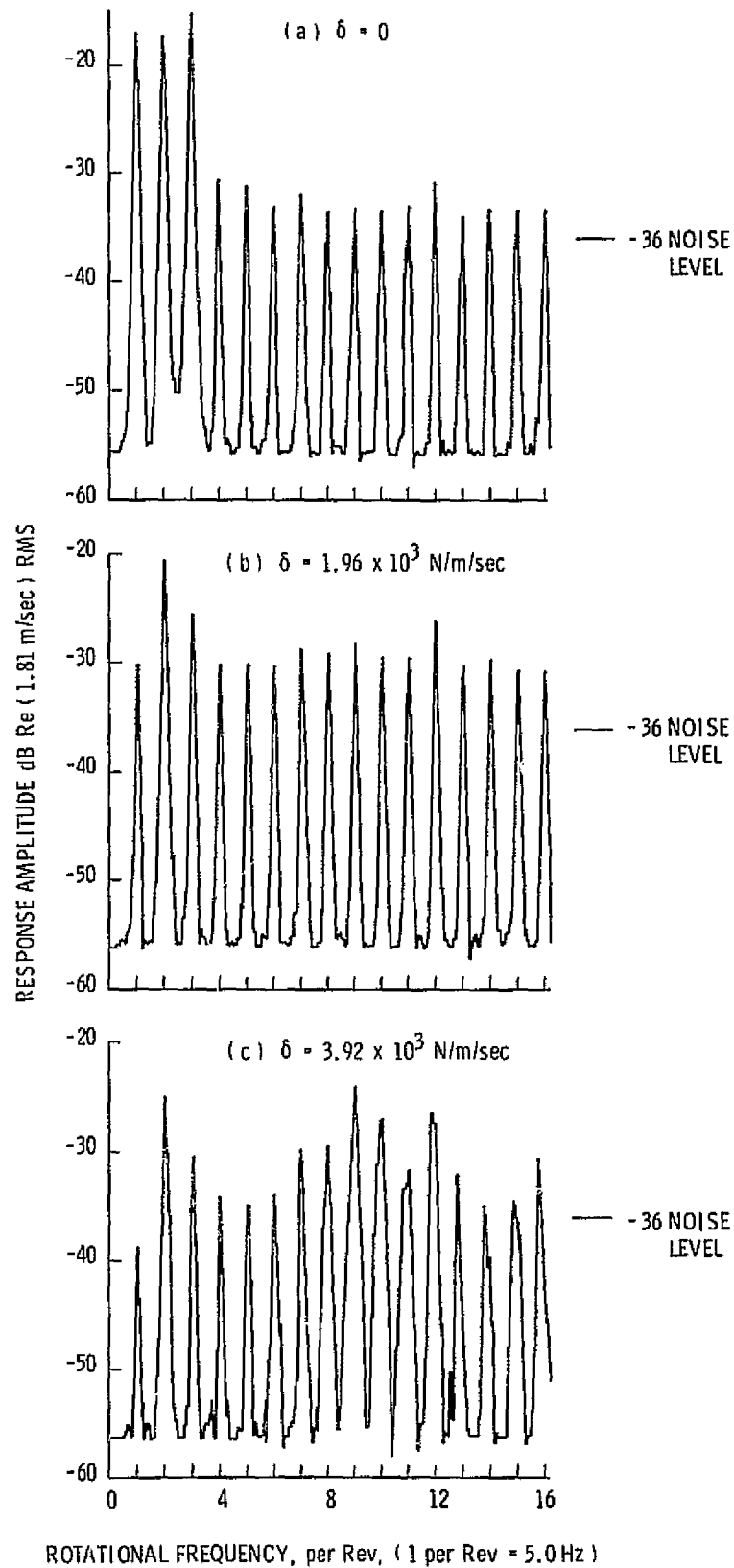
Figure 29. Spectral Plots of V9 Response, μ = 0.26 $v(t)$ = moving pulse, θ_0 = 12°, p = 4
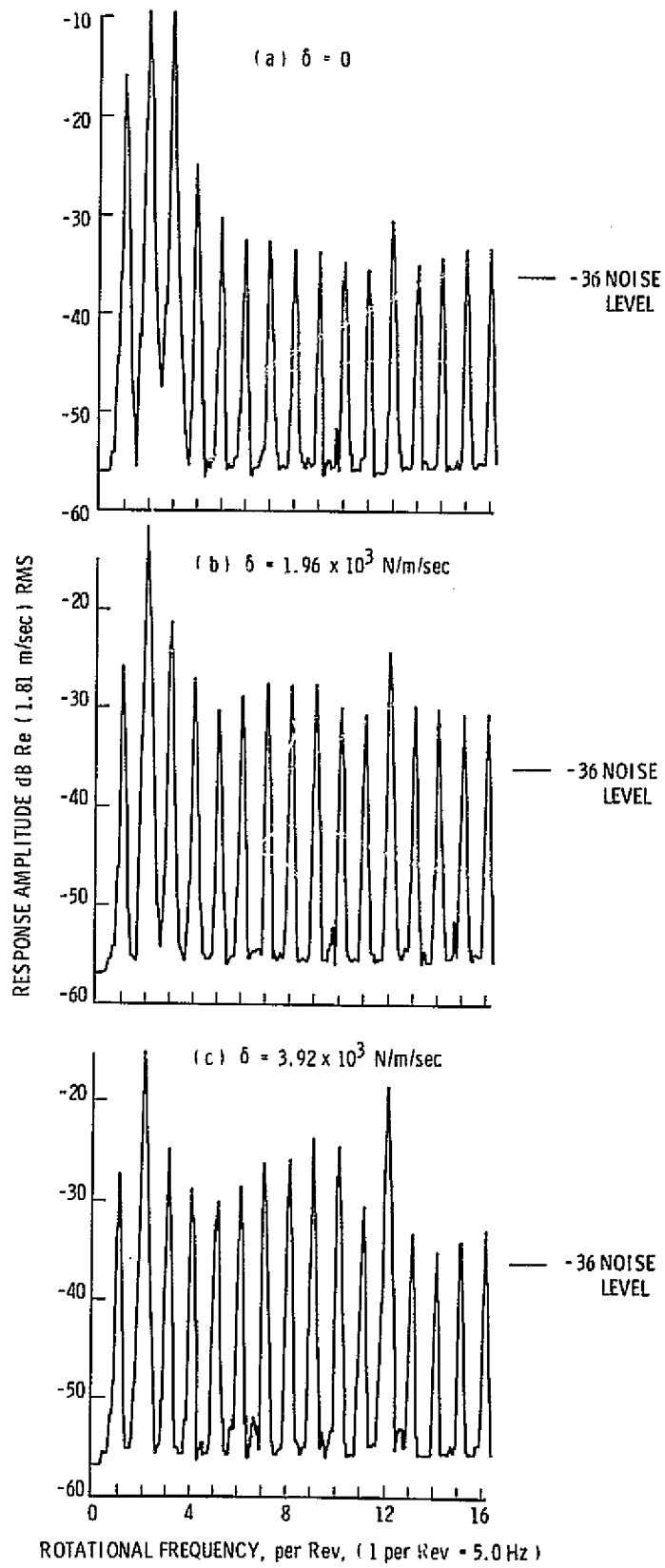
Figure 30. Spectral Plots of V9 Response, $\mu = 0.42$, $\upsilon(t)$ - moving pulse, $\theta_0 = 12°$, $p = 4$

APPENDIX A

RMS and Spectral Response Data

TABLE A-1.   NARROW BAND RMS AMPLITUDE RESPONSE AT V9

(Frequency Range 1 - 10-per-rev)

| μ	δ N/m/sec ×10⁻³	θ₀ = 12°		θ₀ = 11°		θ₀ = 10°	
		V9 m/sec	V9 m/sec	V9 m/sec	V9 m/sec	V9 m/sec	V9 m/sec
		$p = 0$		$p = 0$		$p = 0$	
0.0	0.0	0.068		0.124		0.094	
	1.96	0.019		0.039		0.030	
	3.92	0.009		0.025		0.016	
0.26	0.0	0.317		0.219		0.175	
	1.96	0.192		0.131		0.134	
	3.92	0.131		0.089		0.064	
0.42	0.0	0.782		0.570		0.435	
	1.96	0.490		0.335		0.230	
	3.92	0.315		0.226		0.152	
		$p = 1$	$p = 3$	$p = 1$	$p = 3$	$p = 1$	$p = 3$
0.0	0.0	0.110	0.265	0.232	0.288	0.194	0.279
	1.96	0.078	0.137	0.101	0.138	0.094	0.154
	3.92	0.065	0.238	0.218	0.215	0.138	0.218
0.26	0.0	0.318	0.422	0.309	0.413	0.299	0.529
	1.96	0.213	0.267	0.181	0.223	0.146	0.193
	3.92	0.145	0.296	0.152	0.244	0.168	0.229
0.42	0.0	0.784	0.807	0.610	0.684	0.576	0.625
	1.96	0.499	0.617	0.358	0.390	0.253	0.298
	3.92	0.310	0.467	0.331	0.373	0.218	0.289
		$p = 2$	$p = 4$	$p = 2$	$p = 4$	$p = 2$	$p = 4$
0.0	0.0	0.233	0.310	0.251	0.336	0.215	0.341
	1.96	0.100	0.148	0.107	0.145	0.095	0.155
	3.92	0.081	0.236	0.145	0.201	0.133	0.184
0.26	0.0	0.418	0.483	0.339	0.974	0.356	0.540
	1.96	0.205	0.259	0.215	0.352	0.146	0.201
	3.92	0.158	0.211	0.179	0.234	0.158	0.248
0.42	0.0	0.803	0.918	0.527	0.619	0.617	0.864
	1.96	0.548	0.542	0.333	0.324	0.258	0.291
	3.92	0.338	0.432	0.272	0.242	0.221	0.279

TABLE A-2. NARROW BAND CORRECTED RMS AMPLITUDE RESPONSE AT V9

(Frequency Range 1 - 10-per-rev)

μ	δ N/m/sec ×10⁻³	$\theta_O = 12°$ V9 m/sec	$\theta_O = 12°$ V9 m/sec	$\theta_O = 11°$ V9 m/sec	$\theta_O = 11°$ V9 m/sec	$\theta_O = 10°$ V9 m/sec	$\theta_O = 10°$ V9 m/sec
		p = 0		p = 0		p = 0	
0.0	0.0	0.068		0.124		0.094	
	1.96	0.019		0.039		0.031	
	3.92	0.009		0.026		0.017	
0.26	0.0	0.317		0.219		0.175	
	1.96	0.192		0.132		0.134	
	3.92	0.132		0.090		0.064	
0.42	0.0	0.782		0.570		0.435	
	1.96	0.490		0.336		0.230	
	3.92	0.315		0.228		0.153	
		p = 1	p = 3	p = 1	p = 3	p = 1	p = 3
0.0	0.0	0.065	0.213	0.201	0.240	0.162	0.226
	1.96	0.025	0.060	0.047	0.061	0.039	0.076
	3.92	0.021	0.185	0.177	0.160	0.100	0.159
0.26	0.0	0.286	0.367	0.271	0.358	0.262	0.476
	1.96	0.182	0.200	0.135	0.148	0.096	0.115
	3.92	0.117	0.227	0.112	0.173	0.122	0.162
0.42	0.0	0.754	0.759	0.576	0.632	0.541	0.573
	1.96	0.474	0.562	0.324	0.332	0.212	0.233
	3.92	0.287	0.404	0.291	0.312	0.171	0.217
		p = 2	p = 4	p = 2	p = 4	p = 2	p = 4
0.0	0.0	0.198	0.256	0.220	0.285	0.182	0.285
	1.96	0.045	0.060	0.052	0.058	0.039	0.066
	3.92	0.029	0.175	0.105	0.135	0.092	0.115
0.26	0.0	0.381	0.422	0.302	0.933	0.321	0.482
	1.96	0.164	0.180	0.166	0.300	0.095	0.114
	3.92	0.113	0.135	0.135	0.169	0.110	0.170
0.42	0.0	0.768	0.862	0.495	0.572	0.582	0.789
	1.96	0.514	0.483	0.298	0.277	0.215	0.217
	3.92	0.297	0.361	0.231	0.187	0.171	0.195

TABLE A-3. V9 SPECTRAL RESPONSE AMPLITUDES
For $v(t) = 0$, $p = 0$

$\mu =$	0.0	0.0	0.0	0.26	0.26	0.26	0.42	0.42	0.42
$\delta(N/m/sec \times 10^{-3}) =$	0	1.96	3.92	0	1.96	3.92	0	1.96	3.92

$\theta_o = 12°$ (0 dB = 1.81 m/sec rms)

Rot.Freq. (per Rev.)	-dB	-dB	-dB	-dB	-dB	-dB	-dB	-dB	-dB
1	29.0	42.5	49.0	31.3	42.5	39.0	17.5	27.5	32.2
2	40.0	43.1	49.0	16.0	19.6	23.0	9.3	11.5	15.3
3	47.1			23.2	36.3	40.0	15.8	31.5	41.1
4	50.5			40.3	46.0	52.3	36.2	40.2	42.0
5				50.2		52.3		52.1	49.0
6					52.5		46.2	47.3	49.0
7									52.1
8	52.0								52.1
9					50.2	50.3		47.3	48.5
10						50.3		52.3	47.0
11								52.3	47.1
12	52.0			48.3	50.2	50.3	50.2	52.3	47.1
13						50.3		52.3	47.1
14								54.4	
15								52.2	
16									

$\theta_o = 11°$

Rot.Freq.	-dB	-dB	-dB	-dB	-dB	-dB	-dB	-dB	-dB
1	23.5	35.0	39.9	29.2	43.1	47.0	29.0	39.5	44.4
2	37.7	39.5	43.0	20.0	23.1	26.5	12.3	15.0	18.3
3	49.0	49.0	52.5	24.7	35.6	40.3	14.2	26.1	32.3
4	49.0	49.0	50.4	43.5	50.2	48.6	30.2	41.0	42.4
5	52.8	50.6		48.7	50.0	52.0	41.3	50.0	51.6
6		52.6		52.0	50.0	52.0	45.7	47.0	50.0
7						54.0			51.7
8		52.3	50.8		52.0	52.0		50.0	51.6
9			52.5		48.3			51.7	51.7
10			48.8			52.0		46.9	42.0
11					51.9	47.0	51.6	50.1	45.0
12			52.4	50.2	51.9	43.1	49.7	45.8	39.0
13						48.3			38.1
14						52.0			50.0
15				52.0					
16									

$\theta_o = 10°$

Rot.Freq.	-dB	-dB	-dB	-dB	-dB	-dB	-dB	-dB	-dB
1	26.0	37.3	45.5	26.8	42.0	44.0	23.3	36.4	40.6
2	39.5	41.0	45.8	23.6	26.2	30.0	16.2	18.7	22.0
3	43.0	47.5	50.8	25.5	25.2	40.0	15.5	26.3	32.3
4	52.3		52.6	46.5	52.7	40.7	31.1	42.4	44.8
5	52.3	52.6		50.6	52.7	50.7	47.9		
6				52.7	50.7	52.5	49.0	49.2	47.5
7	52.6			52.7					52.8
8	52.6							50.7	52.8
9			49.0	52.7		50.5		50.7	52.8
10								52.8	43.8
11								52.8	51.0
12	52.7		52.7	46.3	49.0	47.5			44.8
13						52.5			50.7
14	50.6			52.8					
15									
16				52.6					

For $\nu(t)$ = 1 Per Rev, Amplitude 8.47 m/Sec, p = 1

μ =	0.0	0.0	0.0	0.26	0.26	0.26	0.42	0.42	0.42
$\delta(N/m/sec \times 10^{-3})$ =	0	1.96	3.92	0	1.96	3.92	0	1.96	3.92
$\theta_o = 12°$ (0 dB = 1.81 m/sec rms)									
Rot.Freq. (per Rev.)	-dB	-dB	-dB	-dB	-dB	-dB	-dB	-dB	-dB
1	28.0	42.0	46.0	24.6	35.2	40.8	14.2	26.5	32.2
2	36.5	38.7	43.2	16.0	19.2	22.6	8.5	11.4	15.5
3	31.5	40.0	43.5	33.0	52.3	48.6	21.7	34.8	44.4
4	33.8	36.2	40.0	32.0	35.8	40.5	33.6	40.1	44.0
5	39.0	39.2	42.2	37.2	39.0	43.0	36.8	37.8	42.8
6	40.0	37.8	39.5	37.2	37.2	40.8	36.2	37.8	40.7
7	38.0	37.0	39.8	37.2	38.0	41.3	38.3	41.0	47.5
8	39.0	37.0	37.2	37.2	36.3	38.9	37.2	39.0	40.8
9	38.8	35.0	35.0	37.2	36.0	37.3	36.8	38.3	39.6
10	40.0	35.1	35.2	37.2	35.0	35.9	38.2	37.3	37.7
11	39.2	35.3	34.0	36.5	35.0	34.1	37.2	37.2	36.0
12	39.5	36.8	35.1	37.0	34.8	35.0	35.4	36.0	37.7
13	39.5	34.2	30.2	37.0	33.5	31.3	36.3	37.0	34.4
14	38.5	33.8	26.5	36.2	34.0	28.8	37.8	36.2	31.5
15	38.5	35.0	26.0	38.1	34.3	27.8	38.8	37.5	31.5
16	39.0	34.3	25.1	37.3	34.8	26.2	37.2	38.2	30.6
$\theta_o = 11°$									
1	18.5	31.3	34.0	20.6	33.4	39.3	23.5	39.5	40.3
2	33.2	36.5	37.7	20.8	22.5	36.2	13.0	15.0	18.6
3	31.0	39.0	41.0	19.7	30.2	35.1	12.5	23.8	19.5
4	36.2	38.0	41.0	36.1	35.4	40.2	29.0	33.3	36.3
5	36.8	35.0	35.3	34.5	33.5	37.2	33.0	34.5	38.0
6	39.2	36.5	33.6	36.9	34.7	35.7	37.0	34.8	36.0
7	38.0	34.2	31.1	37.3	33.8	34.8	36.0	32.5	34.5
8	40.5	34.9	29.4	37.6	33.3	32.0	37.2	33.0	31.5
9	39.2	35.0	25.5	38.7	33.0	37.7	37.0	32.8	27.1
10	40.2	35.0	20.8	37.6	33.0	23.3	37.5	32.5	23.2
11	40.6	35.5	21.9	39.1	33.7	23.8	38.2	33.0	23.5
12	41.0	36.0	23.0	36.3	33.5	22.6	36.0	32.0	18.6
13	40.1	35.5	22.3	38.7	33.2	24.5	37.5	32.5	24.2
14	40.5	37.0	27.0	39.5	35.0	29.0	38.2	35.0	27.0
15	40.8	37.6	30.4	39.2	34.7	31.0	38.8	34.0	29.8
16	41.5	38.3	33.0	39.5	37.7	33.0	38.2	34.5	31.5
$\theta_o = 10°$									
1	20.3	33.7	39.0	18.9	32.2	36.6	15.7	30.8	33.3
2	33.0	37.0	40.2	24.5	26.0	28.9	17.2	19.2	22.7
3	31.5	39.8	42.5	20.2	30.5	35.5	12.8	24.3	29.3
4	35.9	36.8	41.6	36.0	37.7	39.2	28.0	32.5	35.2
5	37.8	35.7	39.3	36.1	34.7	37.0	33.6	35.5	37.1
6	39.1	37.0	38.3	37.6	34.7	35.6	36.7	34.5	35.0
7	38.4	34.3	36.0	36.8	33.2	33.8	36.1	32.7	33.0
8	41.0	35.7	34.1	38.8	35.0	32.6	37.5	34.0	31.5
9	40.6	34.1	29.0	39.0	33.5	27.5	38.1	33.2	26.7
10	41.0	35.6	24.8	39.2	34.0	24.6	39.0	33.7	24.7
11	40.3	36.3	25.0	40.5	35.2	26.0	38.0	34.3	27.2
12	41.0	36.5	26.8	38.0	35.6	27.4	35.5	32.5	27.5
13	40.8	36.6	27.0	39.3	34.4	27.5	38.3	34.4	30.0
14	41.1	37.3	32.2	37.0	35.4	31.3	39.3	34.5	34.4
15	41.8	37.4	33.8	40.0	36.0	34.1	38.1	35.3	37.0
16	42.5	38.5	36.3	38.9	37.3	36.5	38.6	36.5	39.2

TABLE A-5. V9 SPECTRAL RESPONSE AMPLITUDES

For $v(t)$ - 1 Per Rev Pulse, Amplitude 25.4 m/Sec, $p = 3$

μ =	0.0	0.0	0.0	0.26	0.26	0.26	0.42	0.42	0.42
$\delta(N/m/sec \times 10^{-3}) =$	0	1.96	3.92	0	1.96	3.92	0	1.96	3.92

$\theta_0 = 12°$ (0 dB = 1.81 m/sec rms)

Rot.Freq. (per Rev.)	-dB	-dB	-dB	-dB	-dB	-dB	-dB	-dB	-dB
1	18.4	33.2	37.6	21.5	33.7	34.7	19.5	27.2	29.0
2	32.3	36.6	30.1	16.5	19.5	23.0	10.0	11.0	14.0
3	24.4	34.7	38.6	16.7	27.5	30.7	10.8	22.2	26.2
4	30.7	33.8	36.7	33.2	30.4	31.7	29.5	17.0	28.4
5	33.5	32.4	36.1	32.0	30.2	31.2	30.5	29.3	29.6
6	35.5	32.2	33.7	35.0	29.0	29.7	31.6	28.3	27.5
7	35.6	32.0	32.3	32.7	29.5	27.3	32.4	27.2	26.0
8	35.0	31.0	29.5	33.3	28.7	26.3	33.7	27.1	25.3
9	35.7	30.2	24.0	32.8	28.4	22.7	33.5	28.1	22.7
10	35.5	31.2	19.9	34.3	29.0	20.7	34.8	29.4	21.0
11	36.0	31.9	20.7	34.5	29.5	22.0	35.0	30.5	25.7
12	35.8	33.0	22.1	33.0	26.8	19.0	33.4	26.4	21.0
13	36.0	32.0	23.6	33.6	28.2	27.3	33.1	28.5	35.0
14	36.0	32.2	27.5	34.0	30.0	32.5	34.2	31.5	40.0
15	36.9	33.5	30.2	34.7	31.6	36.7	34.0	31.8	36.9
16	36.8	34.3	32.4	33.4	31.3	38.4	34.7	32.0	33.5

$\theta_0 = 11°$

	-dB	-dB	-dB	-dB	-dB	-dB	-dB	-dB	-dB
1	17.0	31.1	35.4	16.4	30.0	32.3	17.5	33.0	37.8
2	30.7	35.1	37.6	21.0	23.0	25.8	13.0	15.0	18.0
3	26.7	36.2	39.1	17.5	27.4	30.5	11.6	23.0	27.4
4	32.6	34.2	37.8	32.0	31.5	32.2	27.0	29.9	33.3
5	34.2	31.8	35.0	31.0	29.9	31.0	30.0	30.6	33.5
6	34.7	33.2	33.7	33.8	31.0	30.0	32.7	30.1	31.9
7	35.2	31.8	32.5	33.2	29.0	29.1	33.0	27.8	29.3
8	36.0	31.0	29.2	34.1	29.6	26.2	30.4	28.0	26.2
9	36.7	31.3	25.3	34.2	29.6	29.3	33.5	28.6	23.5
10	35.6	31.0	21.0	33.6	28.8	21.6	33.4	27.5	18.2
11	36.3	31.7	21.3	34.2	30.0	24.2	33.6	29.0	20.0
12	37.2	31.5	25.1	33.0	29.3	25.5	32.0	25.7	13.4
13	36.0	31.6	24.5	34.0	30.0	31.5	34.2	27.7	20.8
14	37.0	34.2	31.1	34.1	31.3	40.2	33.6	30.3	24.6
15	36.2	33.3	32.7	35.2	32.0	38.1	33.8	29.8	26.2
16	37.5	35.0	35.1	36.0	33.6	36.4	34.7	31.1	29.3

$\theta_0 = 10°$

	-dB	-dB	-dB	-dB	-dB	-dB	-dB	-dB	-dB
1	17.8	31.2	35.0	15.0	29.1	31.8	14.3	28.0	30.1
2	31.7	35.1	36.5	14.5	25.7	28.9	18.0	18.5	22.0
3	24.7	34.6	36.5	18.3	29.0	31.3	12.1	23.1	27.0
4	31.0	32.4	35.9	31.4	32.3	33.2	27.4	30.2	32.0
5	32.8	31.6	34.8	31.4	30.7	31.5	30.7	31.2	30.5
6	34.5	31.1	32.3	33.0	31.0	30.7	34.0	31.8	30.3
7	34.1	30.0	31.1	33.5	30.2	29.5	34.4	30.0	29.3
8	34.3	30.4	28.6	34.4	30.0	26.7	34.4	29.7	26.3
9	34.8	29.6	24.3	34.1	30.0	34.0	34.9	30.1	24.5
10	35.7	31.1	21.7	34.5	29.8	21.2	35.0	30.0	21.7
11	35.7	31.6	21.8	35.2	30.7	23.6	35.3	31.0	26.2
12	36.5	32.3	25.6	33.6	30.1	25.0	33.1	30.1	26.0
13	34.8	31.4	25.7	34.7	30.1	29.4	34.1	30.0	33.6
14	35.6	32.1	30.2	34.4	31.5	36.0	35.5	31.6	39.2
15	36.8	33.0	34.1	35.7	32.1	38.0	35.0	32.0	35.9
16	36.4	34.2	36.1	35.8	33.0	37.3	36.0	33.1	35.0

TABLE A-6. V9 SPECTRAL RESPONSE AMPLITUDES
For $\nu(t)$ = Moving Pulse, Amplitude 8.47 m/Sec.
p = 2

μ =	0.0	0.0	0.0	0.26	0.26	0.26	0.42	0.42	0.42
$\delta(\text{N/m/sec} \times 10^{-3})$ =	0	1.96	3.92	0	1.96	3.92	0	1.96	3.92
$\theta_o = 12°$ (0 dB = 1.81 m/sec rms)									
Rot.Freq. (per Rev.)	-dB	-dB	-dB	-dB	-dB	-dB	-dB	-dB	-dB
1	19.2	32.0	36.8	17.5	30.6	34.0	17.7	27.3	29.1
2	32.1	35.4	37.0	17.6	20.6	23.8	10.0	12.6	16.0
3	25.8	35.6	38.8	17.8	29.4	33.5	12.0	15.0	27.2
4	34.0	37.5	41.8	34.7	36.0	37.1	18.0	31.5	31.0
5	35.8	36.6	38.2	36.0	35.3	36.7	35.0	35.0	33.1
6	42.8	36.0	41.2	37.1	37.5	35.8	37.6	33.6	32.3
7	37.2	36.2	37.7	36.9	35.2	34.4	37.0	31.5	30.0
8	38.8	36.2	35.8	38.0	35.6	33.7	40.0	34.0	31.0
9	37.2	34.9	35.8	37.8	34.3	33.1	38.7	33.7	29.1
10	38.2	34.0	33.3	37.7	34.3	31.5	40.(	33.8	27.5
11	37.0	36.4	30.0	38.1	33.3	29.3	38.5	35.0	29.4
12	31.0	34.3	38.0	38.8	34.0	32.3	36.2	30.7	27.2
13	38.2	34.5	29.4	37.8	34.1	27.0	39.0	32.6	28.7
14	37.0	34.0	26.7	37.0	32.4	25.5	38.1	32.5	27.3
15	39.0	33.9	23.3	36.5	32.0	23.0	36.8	32.8	25.6
16	39.6	34.0	22.7	37.2	33.0	23.1	38.5	34.0	29.4
$\theta_o = 11°$									
1	18.0	31.0	35.8	19.2	32.3	37.1	22.5	36.4	38.0
2	31.5	34.4	38.0	22.5	24.0	27.3	23.6	16.0	19.0
3	27.5	35.8	39.8	18.0	28.0	33.3	11.5	22.6	27.4
4	37.0	37.3	42.0	34.1	26.5	40.1	26.0	32.4	36.7
5	37.0	35.4	37.9	34.2	24.3	37.3	33.0	36.0	38.5
6	41.0	37.0	39.4	39.2	36.0	37.0	37.5	35.5	36.6
7	37.3	34.0	35.2	36.8	33.3	35.0	36.8	33.5	34.3
8	39.7	35.0	33.2	38.4	34.6	32.6	38.0	32.9	32.0
9	40.3	34.9	29.7	38.0	33.3	28.8	37.6	32.7	28.5
10	41.0	34.3	24.3	38.0	33.6	23.4	37.5	33.0	23.0
11	39.8	34.8	23.5	38.7	33.5	22.5	37.8	32.9	21.5
12	38.0	33.4	24.0	35.2	30.5	20.1	34.0	29.0	15.5
13	40.2	35.5	26.0	37.1	34.5	25.0	29.2	33.7	24.5
14	40.6	37.0	30.5	37.0	34.3	27.9	37.0	33.8	27.0
15	40.1	36.0	33.0	36.1	34.5	30.3	37.6	33.7	29.0
16	40.2	37.5	35.0	37.0	36.0	32.2	38.0	35.0	32.1
$\theta_o = 10°$									
1	19.8	33.5	37.2	16.7	30.5	34.8	14.7	29.2	32.0
2	32.1	35.1	38.8	26.0	27.6	31.3	18.1	19.9	23.2
3	26.7	36.0	40.6	18.8	28.4	33.0	12.0	22.5	27.0
4	35.3	37.5	41.0	33.0	35.0	38.0	26.0	31.7	35.0
5	38.1	36.2	39.6	35.1	35.1	37.5	33.7	35.6	35.5
6	40.5	39.3	39.1	38.2	36.5	36.7	38.4	35.2	34.8
7	39.0	34.6	35.7	36.1	33.7	33.5	36.4	32.7	32.1
8	39.4	36.0	33.4	38.6	34.6	32.2	38.5	33.7	31.0
9	40.0	35.0	29.2	39.0	33.5	27.5	37.9	32.3	26.4
10	41.7	35.4	25.6	38.8	34.1	25.7	39.0	33.0	25.5
11	41.2	36.0	25.0	39.2	35.3	25.8	39.5	34.0	26.8
12	36.8	34.0	25.0	33.2	29.7	22.2	32.2	28.7	21.3
13	43.0	38.2	27.8	38.3	35.4	30.0	40.0	34.5	32.6
14	42.7	38.0	32.7	39.5	36.5	32.2	38.0	34.6	37.1
15	41.8	37.5	34.7	40.0	35.6	34.5	39.0	35.5	39.4
16	40.3	38.3	35.5	39.0	36.6	36.8	37.6	35.0	39.1

TABLE A-7. V9 SPECTRAL RESPONSE AMPLITUDES
For $v(t) =$ Moving Pulse, Amplitude 25.4 m/Sec,
$p = 4, 5$

$\mu =$	0.0	0.0	0.0	0.26	0.26	0.26	0.42	0.42	0.42
$\delta(N/m/sec \times 10^{-3}) =$	0	1.96	3.92	0	1.96	3.92	0	1.96	3.92
$\theta_o = 12°$ (0 dB = 1.81 m/sec rms)									
Rot. Freq. (per Rev.)	-dB	-dB	-dB	-dB	-dB	-dB	-dB	-dB	-dB
1	16.9	30.3	35.0	17.1	30.1	38.6	15.8	25.7	27.0
2	30.7	33.8	37.6	17.4	20.6	24.9	9.5	11.6	14.6
3	22.4	32.7	35.5	15.3	25.5	30.4	9.5	21.1	24.8
4	31.4	32.8	37.0	30.3	30.2	34.2	25.0	27.0	28.8
5	33.7	33.0	35.1	31.7	30.2	34.8	30.3	30.2	30.1
6	36.6	34.0	34.7	33.2	30.7	33.9	32.8	29.0	28.6
7	35.6	30.4	31.8	32.0	28.8	29.8	32.8	27.8	26.1
8	36.0	31.0	29.2	33.7	29.1	29.4	33.6	28.0	25.8
9	36.7	30.7	24.0	33.4	28.1	24.0	33.8	27.8	23.4
10	36.1	31.0	20.2	33.5	29.4	27.0	34.8	29.9	24.5
11	35.5	30.8	19.3	33.0	29.6	31.5	35.5	30.6	30.6
12	35.0	29.7	19.0	30.7	26.2	26.4	30.7	24.3	18.1
13	36.2	33.0	14.6	34.0	30.3	32.3	35.0	29.7	33.1
14	36.0	32.5	18.7	33.5	29.7	34.9	34.3	30.0	35.0
15	35.8	32.5	31.3	33.5	30.7	34.6	33.5	30.8	34.0
16	35.3	33.1	32.0	33.5	30.7	30.6	33.2	30.5	33.0
$\theta_o = 11°$									
1	15.8	29.1	33.5	6.0	16.0	20.6	31.0	37.0	39.8
2	30.0	32.6	36.2	22.3	26.4	29.5	13.0	15.9	19.2
3	23.0	32.7	36.1	15.0	20.5	24.0	12.0	23.6	28.8
4	31.7	34.3	36.1	38.0	36.4	36.0	26.3	34.2	38.5
5	33.2	32.5	35.0	37.2	36.2	34.6	35.0	39.0	42.0
6	36.8	34.5	34.6	37.8	35.8	33.8	40.7	38.0	38.2
7	35.0	31.1	32.0	38.0	36.7	33.3	38.4	34.3	36.0
8	36.4	31.4	29.4	38.0	36.0	32.8	40.7	36.6	34.2
9	37.5	32.2	25.4	37.9	37.6	33.0	40.4	34.7	30.0
10	37.7	31.6	22.3	37.8	37.3	34.4	40.7	36.1	26.0
11	36.0	31.3	22.0	38.4	38.5	35.5	40.2	36.0	25.2
12	33.0	27.7	19.9	31.5	29.0	26.0	34.7	30.5	20.8
13	36.7	33.0	26.5	36.2	35.5	32.0	41.2	37.0	27.7
14	37.7	34.2	33.8	36.2	36.3	33.3	39.6	36.0	29.6
15	36.7	33.6	34.0	35.2	34.9	33.5	38.8	36.0	31.6
16	36.6	34.0	35.5	35.6	36.2	33.6	39.0	36.4	33.4
$\theta_o = 10°$									
1	16.0	29.5	32.6	13.5	26.7	30.0	13.0	26.0	29.0
2	29.5	32.5	36.0	18.0	28.3	31.5	20.0	20.0	23.5
3	22.1	31.7	35.1	16.0	26.0	29.7	19.7	21.5	25.5
4	30.5	32.6	35.2	30.1	31.2	32.5	14.5	29.4	31.0
5	33.2	32.0	34.1	31.5	30.8	31.6	13.3	32.0	30.5
6	35.0	33.4	32.8	35.4	32.0	31.0	14.7	32.7	30.9
7	33.0	30.4	30.2	33.7	29.6	28.7	14.0	30.0	28.2
8	34.7	31.0	28.3	34.5	30.0	27.0	35.1	30.0	26.3
9	35.3	30.1	34.8	34.7	30.0	24.9	35.5	30.3	25.0
10	37.0	32.0	22.8	34.8	30.4	21.3	35.0	30.0	22.5
11	33.9	32.0	23.0	35.3	31.7	26.0	35.8	31.5	29.0
12	25.8	26.0	19.5	30.2	25.6	16.5	30.0	25.5	17.2
13	33.0	33.2	17.8	35.5	31.5	23.5	35.5	30.8	52.5
14	32.4	32.5	32.2	36.0	33.2	41.2	34.9	32.0	38.5
15	32.5	33.4	35.4	34.0	32.2	39.4	34.3	31.5	34.0
16	33.7	33.5	35.7	34.1	32.5	37.1	34.6	32.3	33.0

APPENDIX B

Symbols

SYMBOLS

b	number of blades
c	blade chord, m
C_{DO}, C_{LO}	slope of drag-coefficient versus α and lift-coefficient versus α curves, respectively
e_o	spanwise distance from rotation axis to blade root (eccentricity), m
E	blade elastic modulus, N/m^2
E_o	e_o/R
F_D, F_L	airfoil section drag and lift, N/m
I	blade spanwise bending moment of inertia, m^4
ℓ	blade span, m
m	blade mass per unit length, kg/m
p	identifying number for applied $\nu(t)$ function
Q_{total}	total aerodynamic torque about rotation axis, N-m
Q_x	airfoil section aerodynamic torque about rotation axis, N-m/m
R	$\ell + e_o$, m
t	time, sec
T	airfoil section thrust, $F_L \cos\alpha_r - F_D \sin\alpha_r$, N/m
T_{avg}	Total thrust averaged over one revolution, N
U	relative wind, $\sqrt{U_T^2 + U_P^2}$, m/sec
U_P	total upward velocity in Y_o direction (Figure 1), m/sec
U_T	total velocity, positive in negative Z_o direction (Figure 1), m/sec

V	forward velocity of rotor, m/sec
w	blade deflection at elastic axis, positive downward in direction normal to blade chord, m
x	spanwise position of blade section from rotation axis, m
Z_{ea}, Z_{xo}	positions of airfoil elastic and pitch axis, positive forward of midspan point, m
$Z_{\frac{1}{4}}$	quarter-chord position, positive forward of pitch axis, m
α_r	airfoil section angle of attack, $\theta + \gamma + \phi$, radians
α_s	shaft tilt angle, positive when tilted rearward, radians
γ	elastic torsional rotation about elastic axis, radians
δ	feedback for external damping, N/m/sec
θ	geometric angle of attack, neglecting elastic torsional rotations, with respect to plane perpendicular to rotation axis, radians
θ_c	cyclic pitch amplitude, constant over span, radians
θ_o	geometric angle of attack at blade root (collective pitch), radians
θ_o'	geometric linear twist, positive when θ increases from root to tip, radians/m
μ	advance ratio, $V/\Omega R$
ν	induced velocity, assumed constant throughout disk and positive downward in Y_o direction (Figure 1), m/sec
ρ	air density, kg/m^3
σ	solidity ratio, $bc/\pi R$, m
ϕ	inflow angle, $\tan^{-1} U_P/U_T$, radians
Φ	$\theta + \gamma$, radians
ψ_o	cyclic pitch phase angle
Ω	angular velocity, radian/sec

REFERENCES

1. Bisplinghoff, R. L.; Ashley, H.; and Halfman, R. L.: Aeroelasticity, p. 279. Additon-Wesley Publishing Co., 1955.

2. Etkin, B.: Dynamics of Atmospheric Flight, pp. 280-283. John Wiley and Sons, Inc., 1972.

3. Stepniewski, W. A.: Basic Aerodynamics and Performance of the Helicopter, in Helicopter Aerodynamics and Dynamics. AGARD-LS-63, April 1973.

4. Crimi, P.: A Method for Analyzing the Aeroelastic Stability of a Helicopter Rotor in Forward Flight. NASA CR-1332, August 1969.

5. Kana, D. D.; and Chu, W. L.: Electromechanical Simulation of Helicopter Blade Responses to Random Excitation During Forward Flight. Trans. ASME, J. Engineering for Industry, May 1974, pp. 405-410.

6. Gessow, A.; and Myers, G. J., Jr.: Aerodynamics of the Helicopter, Frederick Ungar Pub. Co., 1967.

7. Scheiman, J.; and Ludi, L. H.: Qualitative Evaluations of Effect of Helicopter Rotor Blade Tip Vortex on Blade Airloads. NASA TN D-1637.

8. Ward, J. F.: The Dynamic Response of a Flexible Rotor Blade to a Concentrated Force Moving from Tip to Root, NASA TN D-5410, September 1969.

9. Kana, D. D.; Yeakley, L. M.; and Dalzell, J. F.: An Experimental Model for Studying Dynamic Responses of a Rotating Beam Under Spatially Distributed Random Excitation. Experimental Mechanics, Vol. 8, No. 9, September 1968.

10. Kana, D. D.: Random Response of a Model Helicopter Rotor Blade. ASME Symposium on Stochastic Processes in Dynamical Problems, Los Angeles, California, November 19, 1969, pp. 41-49.

11. Tanner, W. H.: Charts for Estimating Rotary Wing Performance in Hover and at High Forward Speeds. NASA CR-114, November 1964.